Lawrence Berkeley National Laboratory
LBL Publications

Title
Pulsed-Neutron Method for Detection of Land Mines

Permalink
https://escholarship.org/uc/item/11r9t57t

Authors
Gow, James D
Sinnott, Richard C
Smits, Robert G

Publication Date
1954-12-01

Copyright Information

UNIVERSITY OF
CALIFORNIA

Radiation

Laboratory

BERKELEY, CALIFORNIA

DISCLAIMER

UNIVERSITY OF CALIFORNIA
Radiation Laboratory

Cover Sheet
Do not remove

INDEX NO. _UCRL-2819_

This document contains _22_ pages

This is copy _31_ of _60_ series _A_

Date _December 21, 1954_

Issued to _Information Division_

Each person who receives this document must sign the cover sheet in the space below.

Route to	Noted by	Date	Route to	Noted by	Date

RL-220

DISTRIBUTION: Addresses are not AEC addresses, they have to do with
            a special project
SERIES A 60 copies   1-18-55

Cy. 1/A Mr. Leonard Goff, Commanding Officer, Engineering Research Defense Lab.
         Mine Detection Branch, Ft. Belvoir, Va.
Cy. 2/A Mr. Leonard Goff, ERDL, Ft. Belvoir, Va.
Cy. 3/A Mr. Leonard Goff, ERDL, Ft. Belvoir, Va.
Cy. 4/A Mr. Leonard Goff, ERDL, Ft. Belvoir, Va.
Cy. 5/A Mr. Leonard Goff, ERDL, Ft. Belvoir, Va.
Cy. 6/A Mr. Leonard Goff, ERDL, F^T. Belvoir, Va.
Cy. 7/A Mr. Leonard Goff, ERDL, Ft. Belvoir, Va.
Cy. 8/A Mr. Leonard Goff, ERDL, Ft. Belvoir, Va.
Cy. 9/A Mr. Leonard Goff, ERDL, Ft. Belvoir, Va.
Cy. 10/A Mr. Leonard Goff, ERDL, Ft. Belvoir, Va.
Cy. 11/A Mr. Leonard Goff, ERDL, Ft. Belvoir, Va.
Cy. 12/A Mr. Leonard Goff, ERDL, Ft. Belvoir, Va.
Cy. 13/A Mr. Leonard Goff, ERDL, Ft. Belvoir, Va.
Cy. 14/A Mr. Leonard Goff, ERDL, Ft. Belvoir, Va.
Cy. 15/A Mr. Leonard Goff, ERDL, Ft. Belvoir, Va.
Cy. 16/A Mr. Leonard Goff, ERDL, Ft. Belvoir, Va.
Cy. 17/A Mr. Leonard Goff, ERDL, Ft. Belvoir, Va.
Cy. 18/A Mr. Leonard Goff, ERDL, Ft. Belvoir, Va.
Cy. 19/A Mr. Leonard Goff, ERDL, Ft. Belvoir, Va.
Cy. 20/A Mr. Leonard Goff, ERDL, Ft. Belvoir, Va.
Cy. 21/A Drs. Sylvan Rubin, Samuel Tiamuty, Stanford Res. Institute, Menlo Park,
Cy. 22/A Drs. Sylvan Rubin, Samuel Tiamuty, Stanford Res. Inst.   California
Cy. 23/A Drs. Sylvan Rubin, Samuel Tiamuty, Stanford Res. Inst.
Cy. 24/A Drs. Sylvan Rubin, Samuel Tiamuty, Stanford Res. Inst.
Cy. 25/A Drs. Sylvan Rubin, Samuel Tiamuty, Stanford Res. Inst.
Cy. 26/A Drs. Sylvan Rubin, Samuel Tiamuty, Stanford Res. Inst.
Cy. 27/A Drs. Sylvan Rubin, Samuel Tiamuty, Stanford Res. Inst.
Cy. 28/A Drs. Sylvan Rubin, Samuel Tiamuty, Stanford Res. Inst.
Cy. 29/A Drs. Sylvan Rubin, Samuel Tiamuty, Stanford Res. Inst.
Cy. 30/A Drs. Sylvan Rubin, Samuel Tiamuty, Stanford Res. Inst.
Cy. 31/A Info. Div.
Cy. 32/A Info. Div.
Cy. 33/A Info. Div.
Cy. 34/A Info. Div. Patent Dept -2-7-55
Cy. 35/A Info. Div. UA RL, Livermore 5-17-55
Cy. 36/A Info. Div. Don Wow--10-30-56
Cy. 37/A Info. Div. Dust 1-10-61
Cy. 38/A Info. Div. Dust 1-10-61
Cy. 39/A Info. Div. Dust-1-10-61
Cy. 40/A Info. Div. Dust-1-10-61
Cy. 41/A Info. Div. Dust-1-10-61
Cy. 42/A Info. Div. Dust-1-10-61
Cy. 43/A Info. Div. Dust-1-10-61
Cy. 44/A Info. Div. Dust-1-10-61
Cy. 45/A Info. Div. Dust-1-10-61
Cy. 46/A Info. Div. Dust 1-10-61
Cy. 47/A Info. Div. Dust-1-21-58

Cy. 48/A Info. Div. Dust-1-21-58
Cy. 49/A Info. Div. Dust-1-21-58
Cy. 50/A Info. Div. Dust-1-21-58
Cy. 51/A Info. Div. Dust-1-21-58
Cy. 52/A Info. Div. Dust-1-21-58
Cy. 53/A Info. Div. Dust-1-21-58
Cy. 54/A Info. Div. Dust 1-21-58
Cy. 55/A Info. Div. Dust-1-21-58
Cy. 56/A Info. Div. Dust 1-21-58
Cy. 57/A Info. Div. Dust 1-21-58
Cy. 58/A Info. Div. Dust 1-21-58
Cy. 59/A Info. Div. Dust 1-21-58
Cy. 60/A Info. Div. Dust 1-21-58

UNIVERSITY OF CALIFORNIA
Radiation Laboratory
Berkeley, California

Contract No. W-7405-eng-48

Classification changed to **UNCLASSIFIED**

by authority of $CG \cdot UF-2$: $5.2.3$ ~~

James T. Davis APR 23 1971
SAN Classification Officer

PULSED-NEUTRON METHOD FOR DETECTION OF LAND MINES

James D. Gow, Richard C. Sinnott, Robert G. Smits

December 21, 1954

PULSED-NEUTRON METHOD FOR DETECTION OF LAND MINES

Contents

PULSED-NEUTRON METHOD FOR DETECTION OF LAND MINES

James D. Gow, Richard C. Sinnott, Robert G. Smits

Radiation Laboratory, Department of Physics
University of California, Berkeley, California

ABSTRACT

The detection of land mines by nuclear methods was suggested as
a possibility by scientists involved with design and development of special
weapons. This paper describes the project to investigate the quantitative
possibilities of some of these methods. Two promising detection processes
evolved from the investigation: detection by delayed thermal neutrons and
detection by delayed-capture gamma rays.

A pulsed (d, d) neutron source is placed near a large aluminum
box (18 by 18 by 24 inches) filled with soil or sand. As the neutrons enter
the box they undergo collisions with the nuclei of the soil and are eventually
thermalized. The thermalizing process is most efficiently done when the
fast neutrons from the source collide with hydrogen nuclei present in the
soil or sand. Because mines have a considerable hydrogen content, enhanced
thermal neutron emission and (or) an increase in capture gamma rays emanat-
ing from the soil or sand in which a mine is present provides the possibility
of detecting mines. Obviously, if the hydrogen (water) content of the soil
or sand is equal to or greater than that of the mine, the detection process
fails. The water content of sand and dry soils are such that detection is
possible under conditions described in the report.

PULSED-NEUTRON METHOD FOR DETECTION OF LAND MINES

James D. Gow, Richard C. Sinnott, Robert G. Smits

Radiation Laboratory, Department of Physics
University of California, Berkeley, California

December 21, 1954

INTRODUCTION

At the December 1952 meeting of consultants held at Stanford Research Institute, it was suggested that development work be undertaken on a method of land-mine detection based on the use of pulsed neutron sources.[1] Preliminary measurements were made at the University of California Radiation Laboratory which showed that the method could give detection under certain circumstances. These results were reported at the consultants' meeting held at the Bureau of Standards in Washington in April 1953.[2] As a result, a contract was arranged between the ERDL, Fort Belvoir, and the AEC, to provide funds for further investigation of the method. It was agreed that the work should consist of basic measurements of the magnitude of the detection effects possible under various conditions of soil composition, mine size, and depth. There was no intention yet of designing a field instrument. The development work was aimed at providing the basic data necessary to decide whether a field machine would be practical. The data were also to provide sufficient information to permit some prediction as to the probable performance of a field detector of given specifications. This report states the results of the program.

General Considerations

All methods for detection of buried objects have many features in common. Some source of energy (sonic, radiofrequency, nuclear radiation, etc.) radiates into the earth. Some suitable detector measures the signals reradiated from the bulk of the earth under inspection. The success of such a device is determined by the amount of alteration of the return signal caused by the presence of the buried object. In the general case the detector has an output resulting from the combination of internal noise, external noise, direct radiation from the source, and reflected radiation from the region of soil under investigation.

If there is something that introduces delay between the radiation incident on the material to be searched and the radiation returning to the detector, advantages can be obtained from pulsing the source of radiation and then making the detector sensitive after the source has been turned off. Thus detection of direct radiation from the source may be avoided. If the detector is switched off as soon as the delayed radiation has ended, it may be switched on later into a different channel, which measures the internal and external noise ("background"). This permits a subtraction of these effects from the signal received from the material. Detection consists basically

---

[1,2] See series of reports issued by Stanford Research Institute on Nuclear Methods of Mine Detection.

of measuring a change in the quality of the returned signal, caused by the presence of an inhomogeneity in the material onto which the signal is directed.

The irradiation of material with bursts of neutrons results in delayed radiation. This delay is because of the slowing down and capture processes for free neutrons in matter. If a short burst of high-energy neutrons (~ 3 Mev) is directed into a bulk of material, some neutrons are reflected near the surface and escape. Others enter the material, where they make collisions with the nuclei present. If the neutrons have energies larger than the thermal energies of the nuclei, they lose energy in each collision. The mean free path between collisions depends both on the nuclear composition of the material and on the energy of the neutron. In general, for energies well above thermal, the neutron mean free path is of the order of a few inches. The average fractional energy loss in a collision depends strongly upon the mass of the struck nucleus, and is larger for light nuclei. In hydrogen it is possible for a neutron to lose all its initial energy in a single head-on collision. The average collision in hydrogen reduces the neutron energy to 1/e of its initial value. The average energy loss for collisions with heavier nuclei is much less. The neutrons that enter matter continue to lose energy in such collisions until they reach thermal energies. In this process the average neutron penetrates several mean free paths into the material. After reaching thermal energies, the neutron continues to make nuclear collisions.

For each collision there is a finite probability that the neutron will be captured and incorporated into the structure of the struck nucleus. When this happens one or more γ-rays are emitted in the capture process. There is also a finite chance that the neutron will be scattered back through the surface, into the air. In this case the neutron is lost from the system, since the mean free path in air is very long, owing to the low density. In any event, each neutron will either be captured or lost from the region of interest. Such captures or losses are independent events. If we deal with a large number of neutrons, and measure the number left in the irradiated material as a function of time, we find that they disappear in an exponential manner. This is because the probability of capture or loss is proportional to the number of collisions and the total number of collisions (or losses) per unit time (after thermalization) is proportional to the total number of neutrons present. Thus we have

$$- \frac{dN}{dt} = \lambda N,$$

where $- \frac{dN}{dt}$ is the rate of disappearance of neutrons, λ is the number of collisions per second per neutron times the probability that a capture or escape will occur, and N is the number of neutrons contained in the material. The number of neutrons remaining at any time t after the burst is given by

$$N_{(t)} = N_o e^{-\lambda t},$$

where N_o is the initial number of neutrons delivered to the material. It is not important whether the capture rate or the population be measured, since each is proportional to the other. Because the mean free path and the capture probabilities are functions of the kind of nuclei present, one finds some difference in the neutron disappearance rate as a function of the material. For most soils, however, the constants are such that very little change results

in λ. The inclusion of a small inhomogeneity in such matter does not appreciably alter λ, because most of the neutrons do not chance to traverse it. The quantity $1/\lambda$ gives the mean life of the neutrons in the material, since λ is the probability that they disappear per unit time. In general this mean life turns out to be of the order of 100 to 300 microseconds. This "decay time" provides the delay necessary to permit the use of pulsed sources.

The number of neutrons that thermalize in a given region during the initial slowing-down process depends sensitively on the amount of hydrogen present in the region. This is caused by two effects. One of these is simply that the average energy loss per collision is much larger in hydrogen than for more massive nuclei. The other is that the collision "cross section" for hydrogen happens to be considerably larger than that of most nuclei in the medium- to low-energy range. In Fig. 2 this situation is illustrated. Once thermalized, the neutrons diffuse only a short distance before they are captured. The thermal neutron density is increased around a hydrogenous inclusion. One then finds that this increased density around such an inclusion can be detected either by the increased number of capture γ-rays that come from the inclusion region, or by the increased "leakage" of thermal neutrons caused by the higher density of thermal neutrons around the inclusion.

Clearly all neutrons that do not escape from the material are eventually captured in it. In the absence of a hydrogenous inclusion, however, the neutrons thermalize and diffuse at greater depth. The resulting capture γ-rays, by the time they reach the counter, are attenuated by the increased soil between the capture points and the detector.

Not only the γ-rays, but also the slow neutrons that leak out are attenuated by increased depth. A neutron thermalized close to the surface has a better chance of being detected, as it makes fewer collisions on its way back to the counter. But if they traverse enough material, all the neutrons are thermalized, and in a deeply buried sample any change in distribution caused by the inclusion of hydrogenous material is not apparent at the counter. The return signal at either a γ-ray counter or a slow-neutron counter is found to be larger if a hydrogenous inclusion is located near the source and counter, provided the sample is close enough to the surface to affect the neutron distribution. Further, the magnitude of the disturbance caused by the inclusion is a function of the amount of hydrogen contained.

Since all practical high-explosive materials contain hydrogen, and any plastic case that may be used for mine packaging will probably contain hydrogen, this effect offers a means for detecting the presence of such an object.

In principle, one could calculate the return signals to be expected from such a method of detection. Calculations of the nature needed would, however, be most difficult. Also many of the nuclear constants needed for such calculations are imperfectly known. The practical questions as to the magnitude of the effects seemed best settled empirically, since the necessary experiments are readily done.

Two principal methods of detection of the return radiation were explored in these experiments. One used a sodium iodide scintillation counter

to detect gamma rays coming from the material as a result of neutron capture. With such a counter, it is possible to measure the total number of gamma rays and their distribution in energy. Since practical explosives contain nitrogen, it was hoped that the presence of nitrogen might be detected. This hope was based on the relatively unique spectrum of the capture γ-rays in that element. The amount of nitrogen involved in a buried mine is small indeed compared to the total number of nuclei irradiated. In practice, so few captures occur in the nitrogen that its high-energy γ-rays are unobservable.

The second method of detection of return radiation used a $B_{10}F_3$ neutron counter of conventional design to measure the number of slow neutrons diffusing out of the surface of the material after it had been impregnated with a high-energy burst of neutrons.

For both detection methods only one factor was found to appreciably influence the amount of radiation received by the counters after a neutron burst. This was the presence or absence of hydrogen. As is seen in the section giving the detailed experimental results, in all cases the presence of hydrogen increases the amount of returned radiation. It appears to be quite immaterial what the composition of the hydrogen-containing compound is. The presence of water in soils interferes with this type of detector. The detection ratios (ratio of returned radiation from soil containing a mine to returned radiation from soil not containing a mine) fall steadily with increasing water content. At something like 15 to 20% water (by weight) the detection effects vanish into the general background. As long as the hydrogen content of the mine is appreciably different from that of its surroundings, it is detectable. For most situations involving sand, the mine will still contain more hydrogen than the soil, since sand becomes saturated with water at a content of about 3% weight. For soils of the adobe or loam type the water content may vary between 10% and 40%. In this case the detector will operate only at the lower water concentrations.

For a mine detector of this type to be practical, two criteria must be satisfied. First there must be an appreciable change in the returned signal caused by the presence of a mine. Second, the returned signal must have a reasonable amplitude for practical values of source strength. A detector that changed its output from 1 count/10 hours to 1 count/hour in the detection process would have excellent signal/noise ratio but detection times would be ridiculously long. When the statistical nature of the returned signal is combined with the actual counting rates obtained, the detection times are determined entirely by the necessity of accumulating sufficient counts to make the statistical variations small in comparison to the changes caused by the presence of the mine.

EQUIPMENT AND PROCEDURES

Mock High Explosive, MHE

For most of the experiments reported here the buried sample con-
sisted of an "artificial" high explosive. It was found that a mixture of car-
bon, in the form of graphite, and ammonium nitrate could be chosen that
closely simulates the average chemical composition of the common high ex-
plosives. The sample was compounded of 37% by weight of carbon, 63% by
weight NH_4NO_3. This gives the following percentage atomic composition:
hydrogen 31.3, carbon 29.7, nitrogen 15.6, and oxygen 23.4. This mixture
is henceforth referred to as MHE. The samples were sealed in small card-
board containers, which were waterproofed with tape and plastic spray.
This treatment was necessary to prevent the ammonium nitrate from absorb-
ing water from the air or soil.

For one set of experiments a "special sample" was used. It was a
small mine case (M-14) filled with MHE. In order to demonstrate that the
method responds only to the presence of hydrogen, some other runs were
made using buried hydrocarbons, water and blocks of carbon, aluminum,
and a dewar containing liquid nitrogen. Significant changes in the counting
rate of the detector counter relative to the source monitor were produced
only by the hydrogen-containing samples. The magnitude of the detection
effects was in all cases closely proportional to the amount of hydrogen in
the sample.

Experimental Setup

For all experiments (both systems of detection) only one basic ge-
ometry was used. The neutron-producing target of the accelerator (see Ap-
pendix I) was placed in close proximity to a large aluminum box (24 by 18
by 18 in.). This box was filled with the type of soil under investigation.
The counter that was to detect the radiation returned from the soil was placed
to the side of the target. For gamma counting with the NaI counter, lead
shielding was placed between the target and the counter to reduce direct ac-
tivation of the counter by fast neutrons. For the thermal-neutron detection,
no such shielding was used.

The general procedure consisted of making measurements of the
total counts accumulated by the detector counter during the irradiation of
the earth with a known number of fast neutrons. Such measurements were
made with the box containing only earth, or earth plus a measured amount
of MHE at the desired depth. In γ-ray counting, an additional variable is
the spectral distribution of the γ-rays. For this method it was necessary
to investigate the counting rate per unit energy interval for various samples
and sample positions.

DETECTION BY COUNT OF DELAYED THERMAL NEUTRONS

The geometry used for the detection of buried explosives by delayed thermal neutrons is shown in Figs. 1 and 4. Two identical counters were used, both being standard $B_{10}F_3$-filled neutron counters. One of these (monitor counter) was placed ~ 3 feet from the accelerator target and surrounded with a paraffin moderator. This counter served to monitor the output of the neutron source. It was calibrated in approximate number of neutrons per count by means of a standard PoBe neutron source that could be placed near the neutron-producing target. The detector counter was placed alongside the neutron-producing target. As far as practical, any material that might retain thermal neutrons was kept away from this counter. The counter signals were amplified and delivered to standard UCRL gated scalers. Two scalers were provided for each counter. The times during which these scalers could record counts were controlled by a scaler gating unit (see Figs. 5 and 6).

The neutron source was pulsed at 60 cps and adjusted to give a 200-μsec burst of neutrons. After a delay of 25 μsec from the end of the neutron burst, the detector signal scaler was turned on and kept sensitive for 300 μsec. After further delay of 6,542 μsec the detector-counter signals were counted for 600 μsec into the detector-background scaler. Since by this time all the neutrons produced in the burst would have been captured, the detector-background scaler recorded only counts resulting from stray radiation. The number of counts on the detector-background scaler was divided by 2 before subtraction from the detector signal scaler count since the detector background scaler is gated "on" twice as long as the detector signal scaler. At the end of this 600-μsec period, the monitor counter background scaler was gated on. This gate remained open for 8,333 μsec. The monitor-signal scaler was allowed to count throughout the time. Thus the background for the monitor counter was measured during the last 8,333 μsec of the 16,667-μsec period of the pulsing sequence. (A 667 μsec period at the end of the sequence was left to insure that the neutron background scaler gate would not drift into the region of the neutron pulse.) Again assuming all the neutrons produced in the burst have been captured in the first few hundred microseconds, this background signal multiplied by 2 gives the actual background, which must be subtracted from the neutron monitor count to get a net count proportional to the true neutron output. The timing sequence is shown in Fig. 6.

The choice of the length of time for which the detector-signal scaler is to be made sensitive is a compromise between obtaining the maximum number of real counts and leaving it sensitive so long that appreciable background counts are included. This time was chosen by first measuring the apparent decay rate of the signal in this counter after the fast-neutron burst. This was done for SiO_2 sand with 2% (by volume) water content. To make this measurement, the gate width for the detector-signal scaler was set at 100 μsec and the gate moved to various times after the neutron burst. The number of counts for a constant neutron irradiation of the sand was recorded and plotted as a function of time (Fig. 7). The apparent half life is 215 μsec. When the detector-signal scaler counting time is set at 300 μsec substantially all of the signal is recorded.

OBSERVATIONS AND INTERPRETATION

Detection Ratio

The experiments with this system consisted of the burial of samples of MHE at various distances from the counter in various soils. The change in the net detector counting rate relative to the net monitor counting rate caused by the sample was measured. In order to express the data in simple form, two quantities are used. One of these is the detection ratio. This is defined as the change in net detector counting rate relative to the net monitor counting rate caused by the introduction of the sample into the soil.

Let M_F be the total monitor counts minus background accumulated during a run (i. e. , the outgoing neutron flux) and M_T be the total counts minus background accumulated by the detector counter (the thermal neutrons returned to the detector) during the same run. The detection ratio is defined

$$\text{DR} \equiv \frac{\dfrac{M_T}{M_F}(\text{sample in})}{\dfrac{M_T}{M_F}(\text{sample out})} .$$

When there is no detection DR = 1. When a sample is introduced, the DR becomes >1. The change in the net detector counting rate relative to the net monitor counting rate caused by inserting the sample may be usefully expressed as percent detection $\equiv$ (DR - 1) x 100. This quantity is plotted in Figs. 8, 9, 10, and 11 for dry sand (est 1/4% H_2O by volume), sand containing 5% water by volume (substantially saturated), and dry adobe soil. The adobe was analyzed by Stanford Research Institute and proved to have a total H_2O content of 9.8% by weight (free, 5.6%; bound, 4.2%). The samples used in these measurements are as shown on the graphs. For all these measurements the sample was placed directly in front of the counter, as shown in Fig. 13.

For all the data shown in Figs. 8, 9, 10, and 11, the deuterium target and the counter were spaced approximately 2 inches from the front surface of the box.

One expects some variation in the counting rates and detection ratio as the counter and target are moved away from the surface of the soil. This effect was investigated by measuring these quantities as a function of the distance of the machine from the soil surface. Figure 12 is a plot of the variation.

These runs were made for a fixed sample depth chosen to give a high detection ratio. It is seen that there is a fairly rapid variation in the spacing range of one to three inches. The curve becomes rather flat thereafter. In a field machine one would have to choose a compromise distance that could be held in practice.

It is also of interest to know how fast the signal falls off as the sample moves away from the center of the counter. A set of runs at constant depth was made in which the sample was placed at various positions. These data are plotted in Figs. 13 and 14.

Searching Rates (Mathematics)

The time required for searching a given area with this method is fixed by the statistical nature of the returned signal. It is obviously necessary to accumulate sufficient net counts from the detector counter to assure that any variations in rate observed are real and not statistical fluctuations. The following analysis gives the times that would be required for detection with a machine having properties similar to the equipment used in the laboratory investigations. Also included are the scaling laws, which will permit extension of the data to other sets of specifications. (See Appendix III.)

The searching time is a function of many related variables. Among the variables are neutron flux from the machine, net number of counts (per unit time) recorded from counters with sample in and sample out, detection ratio, and the chance that a negative indication may occur even though a mine is present. We must recognize the statistical nature of these measurements; the interrelations between the variables may be illustrated quantitatively as follows.

The detection ratio DR is a ratio of M_T/M_F with sample in to M_T/M_F with sample out, where M_T and M_F are the net number of counts from detector and monitor. Let us designate the net number of detector counts with the sample in as M_{Ti} and with the sample out as M_{To}. The higher the number of counts in any counter the lower the error; as the counting rate of the flux monitor counter can for all practical purposes be made as high as one wants, we can safely assume that we know M_F exactly. If we set the conditions so that M_F with sample in is no different from M_F with sample out, then DR becomes simply M_{Ti}/M_{To}.

From statistical procedure we know that the fractional probable error in M_{Ti} is $0.67/\sqrt{M_{Ti}}$ and in M_{To} is $0.67/\sqrt{M_{To}}$, so the fractional probable error in DR is therefore

$$\sqrt{\left(\frac{0.67}{\sqrt{M_{Ti}}}\right)^2 + \left(\frac{0.67}{\sqrt{M_{To}}}\right)^2}.$$

We can designate this as f_{DR}.

Let us also set the conditions so that counting time with sample in is the same as counting time with sample out. Then $M_{Ti} = DR\ M_{To}$ so:

$$f_{DR} = \sqrt{\left(\frac{0.67}{\sqrt{(DR)M_{To}}}\right)^2 + \left(\frac{0.67}{\sqrt{M_{To}}}\right)^2}$$

Then: $f_{DR} = 0.67\sqrt{\dfrac{DR + 1}{DR\ M_{To}}}$ but: $\dfrac{M_{To}}{R_{To}} = t$ where R_{To} is the counting rate with no sample and t = time.

then: $f_{DR} (R_{To}t)^{1/2} = 0.67 \sqrt{\dfrac{DR + 1}{DR}}$.   (1)

From the above equation, we can determine how long we must count to get a certain fractional error f_{DR}. A plot of $f_{DR} (R_{To}t)^{1/2} = F(DR)$ vs DR is given in Fig. 43.

Detection Factor

The above equation is calculated using the fractional error (f_{DR}) because it fits the type of calculation very nicely. Another method of indicating error lies in the probable error, called E. This error defines the limits of a statistical number, such as the detection ratio, so that the value given ± the probable error, E, will have a 50-50 chance of including the true value of the number. If the detection ratio is given as $1.5 \pm .1$, the probable error (E) is 0.1 and there exists a 50-50 chance that the true value of the detection ratio is between 1.4 and 1.6 or is greater than 1.6 or less than 1.4. However, the chances of the number's being much less or much greater than the given number become progressively less as the deviation from this number (1.5) becomes larger.

The relationship between E and f_{DR} is indicated as follows:

$$(DR)\, f_{DR} = E .$$

At this point it is advantageous to define a quantity that will describe the relationship between the chance of a large deviation vs the amount of the deviation (error). This quantity is called the detection factor, DF, and is related to the probable error (E) and the detection ratio DR. Thus,

$$DF = \frac{DR - 1}{E} ,$$

and is also related to the fractional error, f_{DR},

$$DF = \frac{DR - 1}{(f_{DR})(DR)} .$$

It will be noted that the smaller the fractional error (f_{DR}) or the probable error (E), the larger the detection factor DF. A graph of odds against "no detection" vs detection factor is given in Fig. 44. It must be kept in mind that the detection factor is a number describing the "safety" of a given search, and as such is subject to the choice of the designer of the machine. The detection factor, by putting limits on the errors, influences the time required for detection. A sample calculation is given in Appendix III which indicates the use of the detection factor.

Searching Rates (Counter geometry)

So far we have discussed the interdependence of detection time and detection ratio (DR), fractional error (f_{DR}), and detection factor (DF). The time is also a function of neutron flux from the source, number of counts recorded from the counters, and the machine geometry. The arrangement

we used for collecting data had one BF_3 counter* to detect thermal neutrons from the box (detector counter). This counter would "look at" an area of approximately 0.5 ft.². If two counters were placed next to each other and connected in parallel, the counting rate would double and an area of about 1 ft² could be observed by the counters. With four counters, an area of 2 ft² and four times the counting rate could be observed, etc. At this stage, however, an analysis of what is happening to the % of detection [(DR - 1) x 100] is important.

Reference to Figs. 13 and 14 shows how the percent detection varies as the sample is moved to various positions, with respect to a counter and the source, but is kept at constant depth. Taking the data for one counter while moving the sample around is equivalent to moving the source and counter over the sample. It will be noted that, for the planar run (Fig. 13), the percent detection does not change radically over the range observed. If the sample were placed in Position 3 but on the other side of the source, the percent detection would be zero (or very nearly so). If, then, we had a set-up such as that in Fig. 3 but with all 12 counters connected in parallel, and a mine directly under the counters on the right side, no detection would be sensed by the left side and the net percent detection would be half of the maximum possible percent detection. The answer to this problem would be to have each set of four counters operate into separate indicating devices. Because the source radiates isotropically we may place these sets of counters as shown to most efficiently utilize this symmetrical radiation. Figure 14 shows the variation as the sample is moved along a line perpendicular to the axis of the BF_3 counter. The sets of four counters were chosen so the areas observed would be approximately square and would smooth the more rapid variation shown in Fig. 14.

Even with the sets of four counters the percent detection is reduced somewhat if the mine is not centered. About all that can be done, at this stage, is to make an educated guess at the reduction. If a mine in the shape of a 2-inch cube (like our sample) were centered under the end two counters, the net percent detection would be about 25% less than in the ideal case with only one counter and the mine exactly centered.

Under the conditions described above, with three sets of four counters each for the detectors, the time for "looking at" 6 ft² (2 ft² per counter set) would appear to be reduced to 1/4 of the values listed in Figs. 15, 16, and 17 (with only one counter). This reduction is due to the linear relationships between the counting rate and the number of counters. The reduction in DR, however, does not show a linear relationship to the amount of time needed for detection, but goes approximately as the square (refer to Eq. (1) page 13), and increases the time needed for detection by a factor of about 1.6. Thus the searching time listed in the graphs would be reduced by a factor of about 1.6/4 or about 0.4. A 100-second searching time with laboratory equipment would be reduced to 40 seconds with the above-described equipment.

If, in addition, source strength were increased by a factor of 10, this time would be reduced to one tenth, or 0.04 sec, because this is a linear relation. If a further tenfold increase in the strength of the source** could

---

*The particular counter used had an efficiency of 2%.
**The time graphs, Figs. 15, 16, 17, 25, 26, and 27 are based on a source
  intensity of 10^6 neutrons per second, average.

be obtained (10^8 neutrons per second), the times would be reduced by another factor of 10, and so on.

The counter efficiency is about 2%. If, by increasing the volume, density, etc., of the counters, a gain of 10^1 in the efficiency could be obtained, then another reduction of ten in the search time would be achieved. The search times would now be reduced to 1/2500 of the time with laboratory equipment. (Assuming that the methods of increasing the efficiency of the counters would not affect the geometry sufficiently to reduce the percent detection by more than a factor of 25%, as mentioned previously.) A laboratory search time of 1000 seconds would be reduced to 0.4 second, with a search area of 6 ft.^{2} and a linear dimension of 2 ft. The vehicle carrying a detector could now move at a rate of 2 ft. per 0.4 second or 3.4 miles per hour.

It must be kept in mind that the above discussion is based on extrapolations of the data accumulated in the laboratory, and is subject to experimental verification with a field model. Some of the extrapolations are well justified (time vs neutron flux, time vs counting rate), while others are more in the realm of an "educated guess."

Special Experiments

The possibility that the detector counter might have a high background count due to thermal neutrons reflected from the walls of the room and therefore show lower detection ratios than might be obtained in the field was checked in the following manner: A curved piece of 1/16-inch cadmium sheet was placed in back of the detector counter on the room side (i.e., away from the wall). By this placement, any thermal neutrons directed toward the counter, other than from the "sandbox", were captured in the cadmium. The detection ratios were unchanged by the addition of this shield, and it was therefore demonstrated that the neutrons counted were coming principally from the "sandbox".

A carbon block (3 by 3 by 6 inches) was placed at a 2-inch depth in sand + 5% water by volume to see if the carbon in the MHE had any effect on the detection ratios. The percent detection for this case went slightly negative, indicating that the carbon was a somewhat less effective moderator than wet sand.
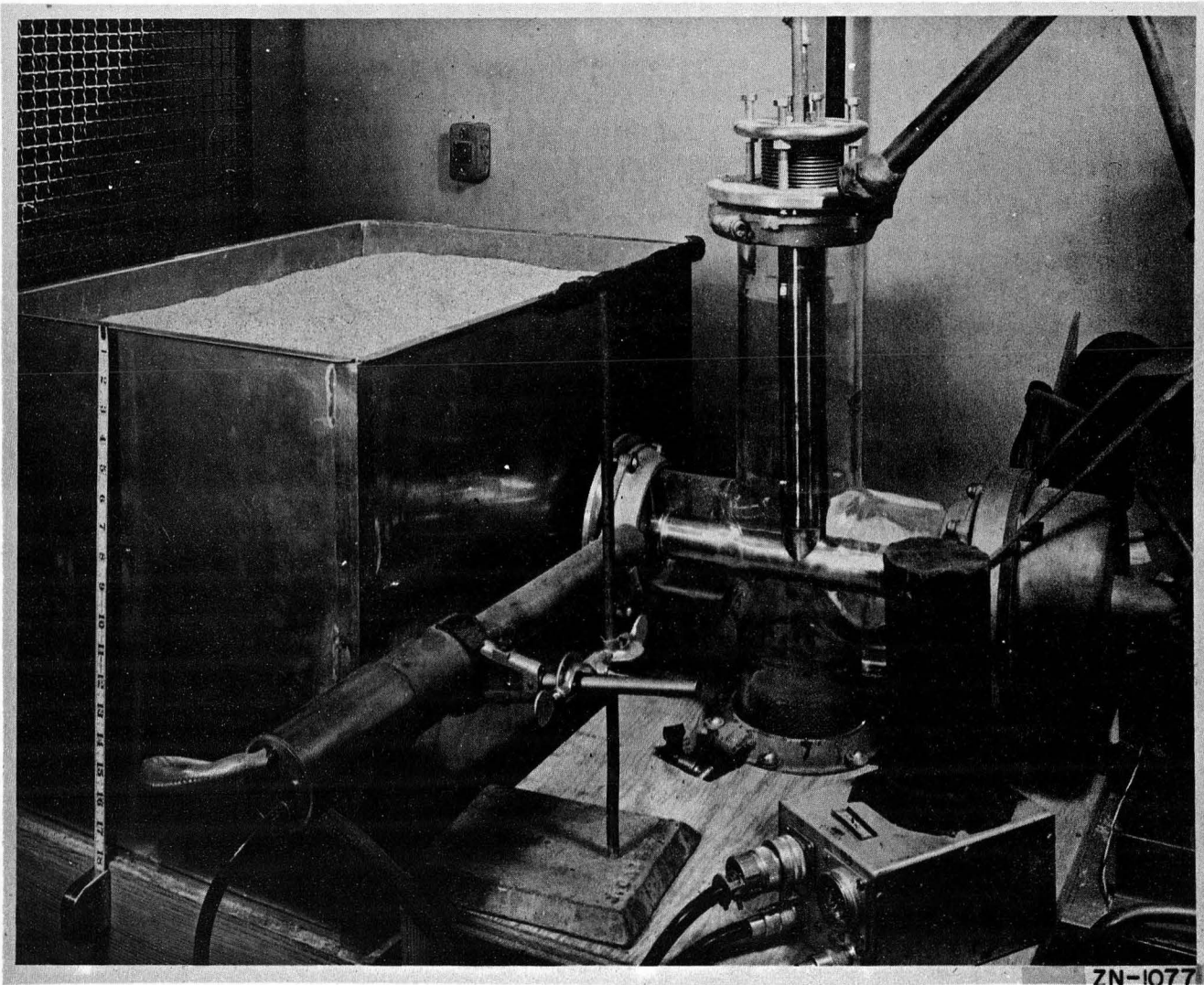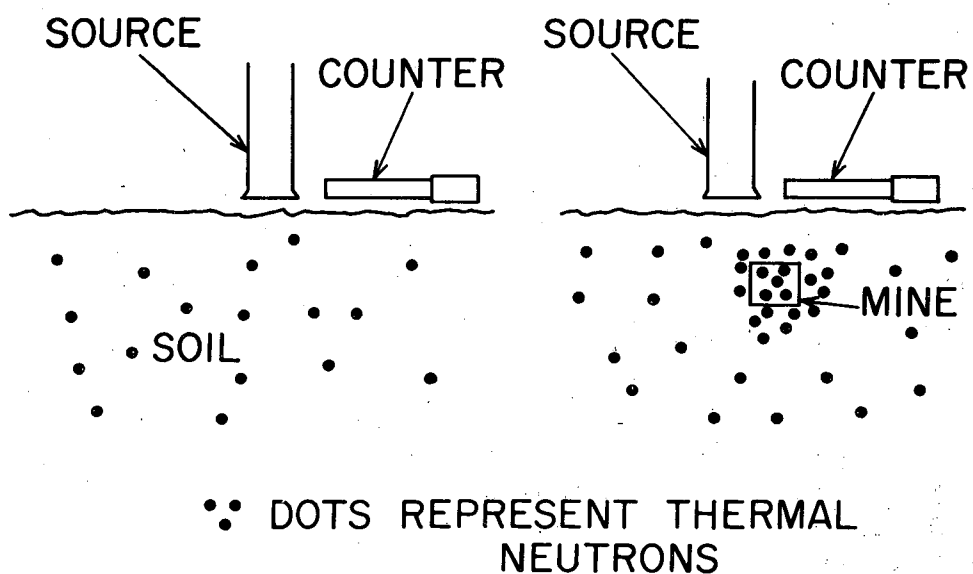
Fig. 1. Neutron-counter orientation.

SOURCE   COUNTER   SOURCE   COUNTER

DOTS REPRESENT THERMAL
NEUTRONS

FIG. 2

MU-8771

Fig. 2. Neutron distribution in soil.

3 SETS OF 4BF₃ COUNTERS
EACH

SOURCE

TO COUNTER
CIRCUITS

SEARCH AREA
APPROX. 6 sq.ft.

DIRECTION OF SEARCH

FIG. 3

1½" DIAMETER

SOURCE   SENSITIVE AREA

8"   BF₃ COUNTER

TARGET

2"

12"

15" OR 16"

USEFUL   RADIUS
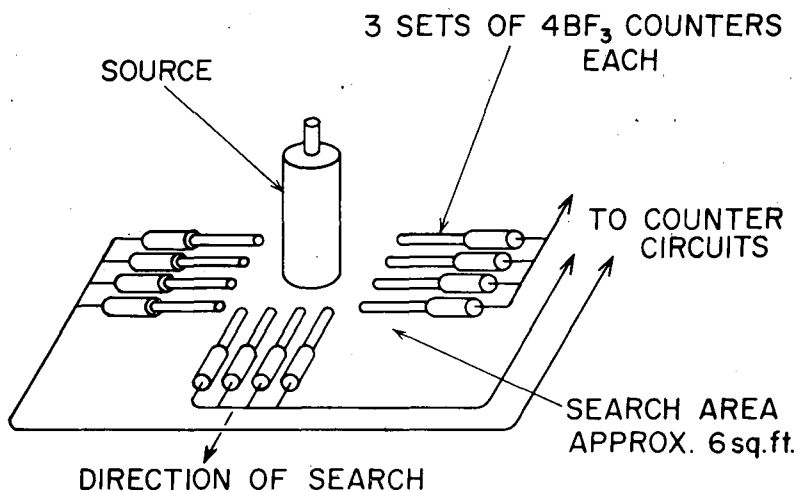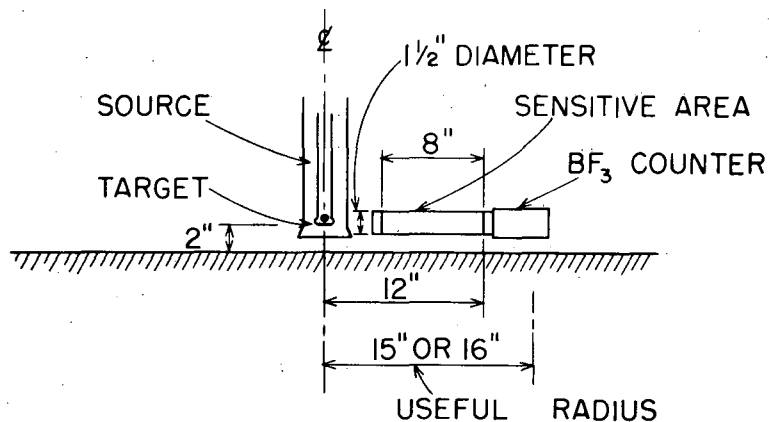
FIG. 4

MU-8772

Fig. 3. Possible geometry of field counter.

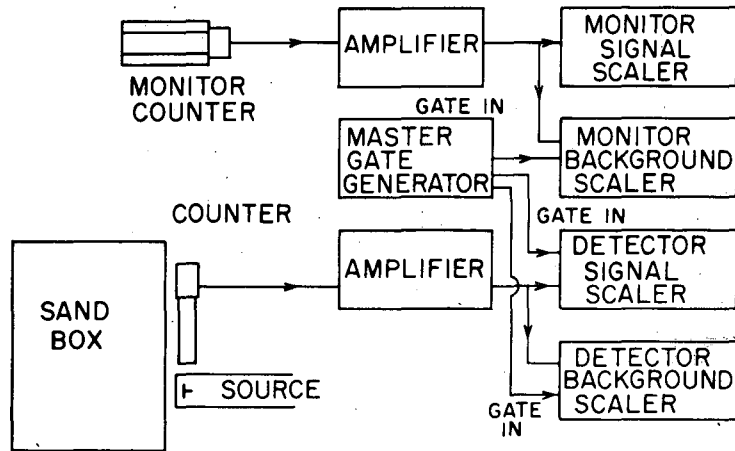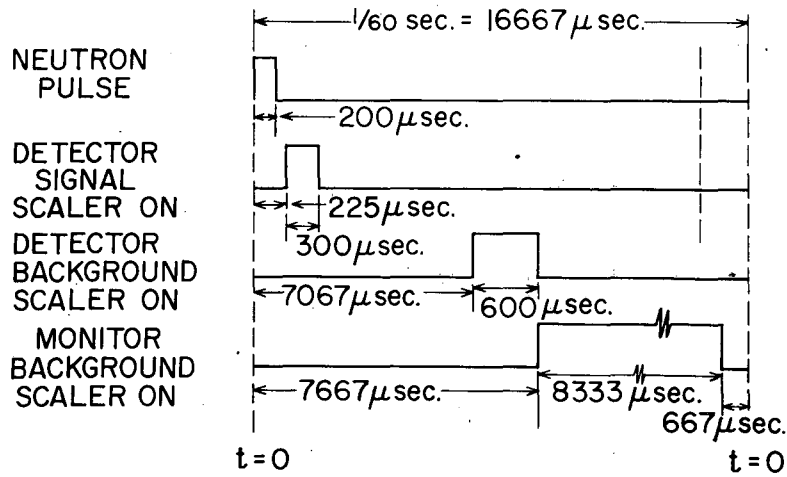Fig. 4. Dimensions of neutron-counter geometry (laboratory
   arrangement).

FIG. 5

FIG.6

MU-8773

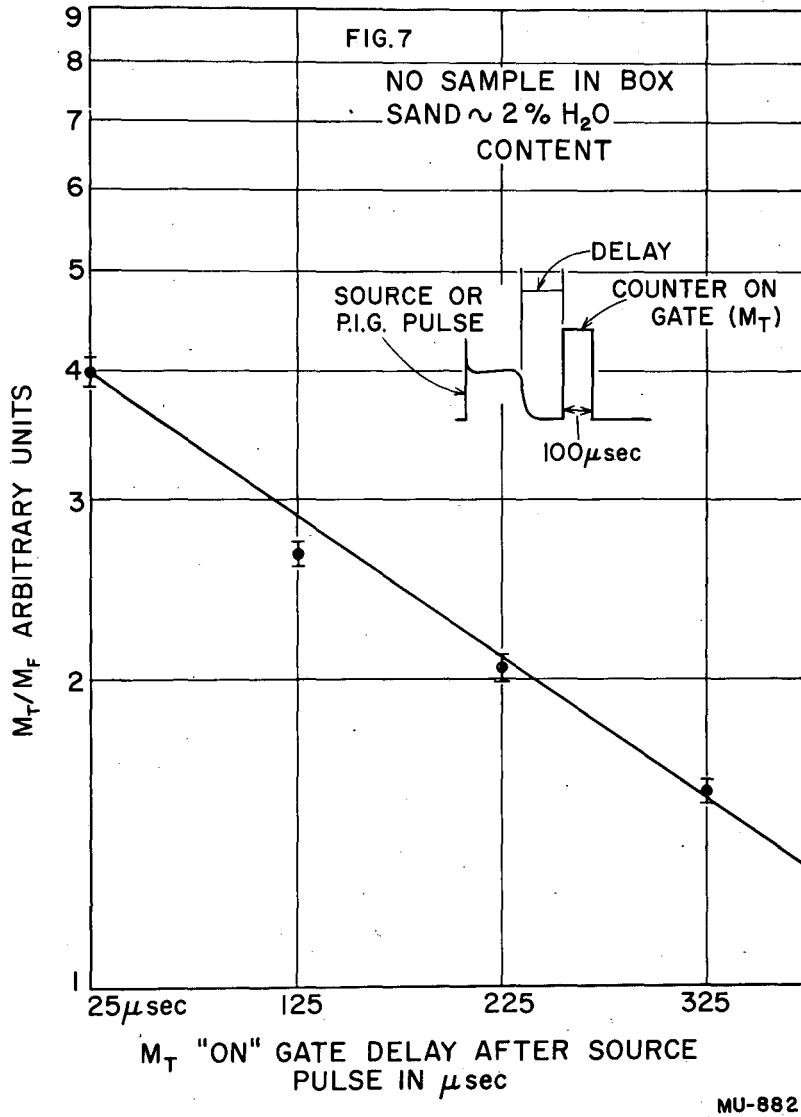Fig. 5. Block diagram of neutron-detection system.

Fig. 6. Gating sequences.

Fig. 7. Neutron "half life" (graph).

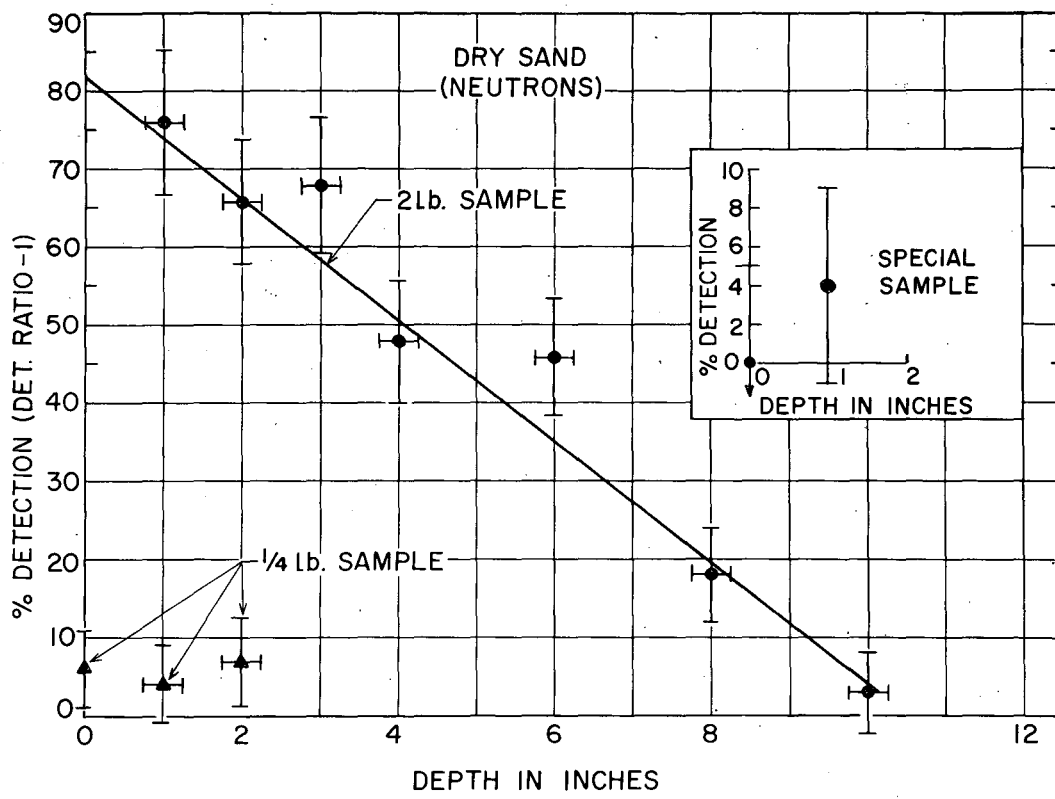Fig. 8. Percent detection vs depth for dry sand.

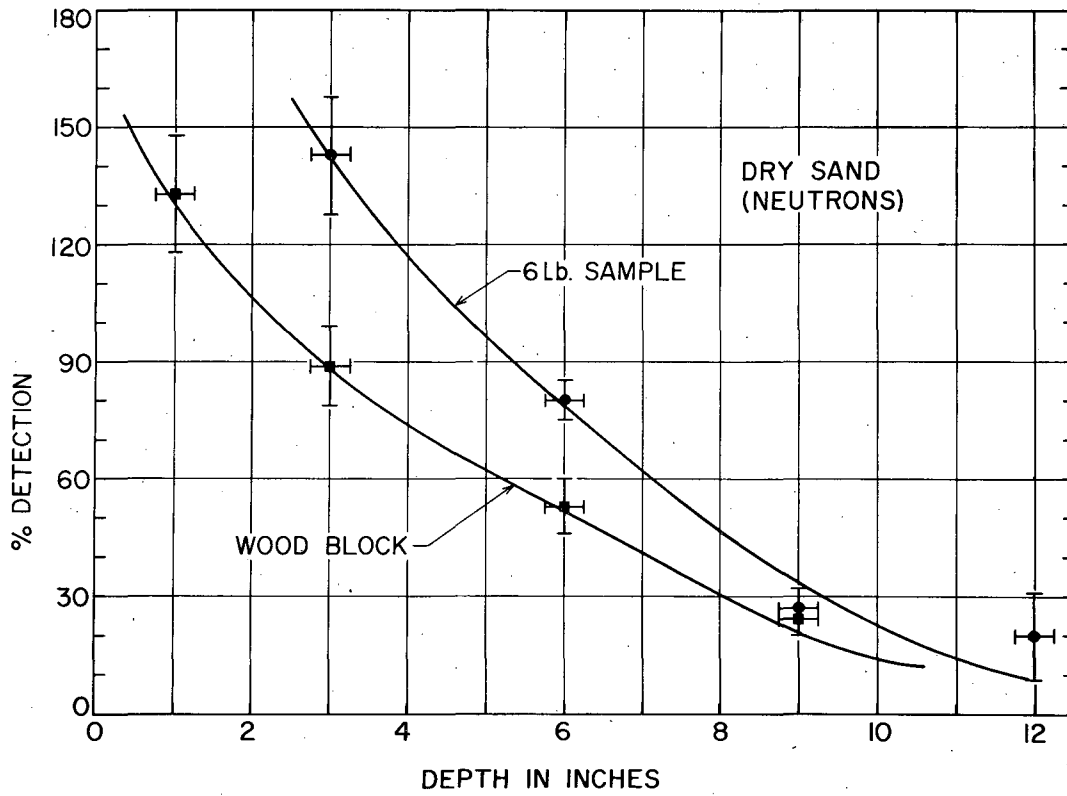Fig. 9.   Percent detection vs depth for dry sand.
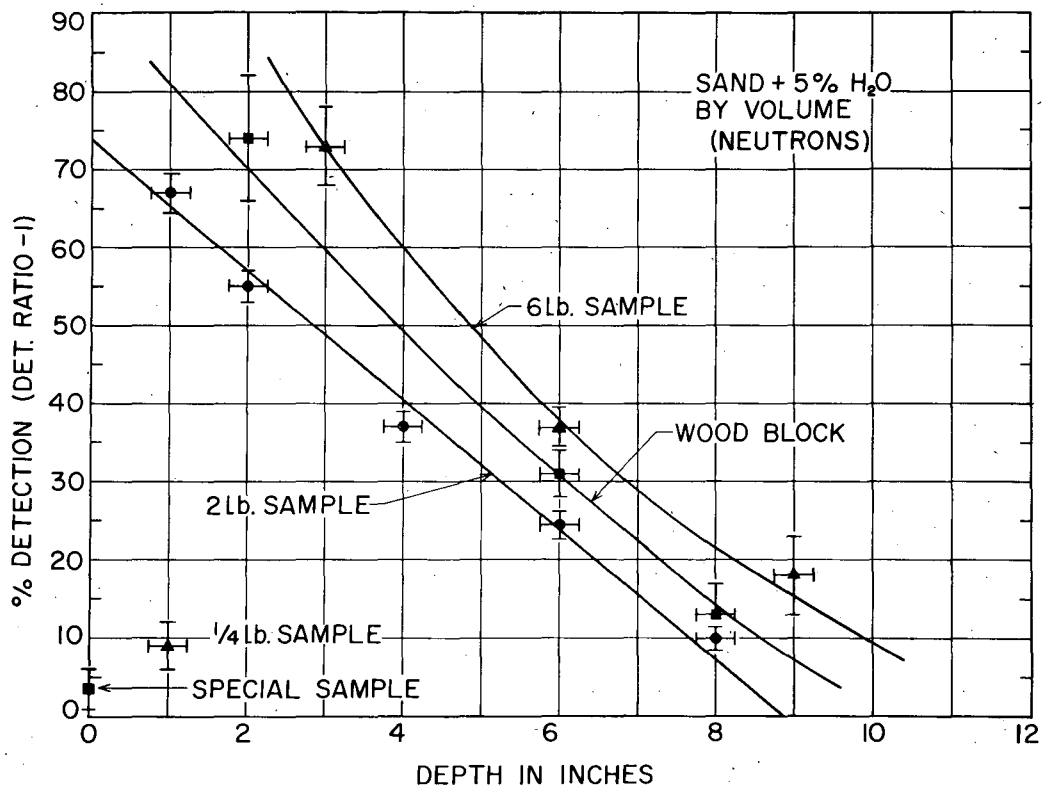
Fig. 10.   Percent detection vs depth for wet sand.

Fig. 11. Percent detection vs depth for dry adobe soil.

EARTH TO COUNTER &
SOURCE VARIATION (NEUTRONS)
SAND WITH 5% H_2O
BY VOLUME
2 lb. SAMPLE AT 1" DEPTH

% DETECTION

$\frac{M_T}{M_F}$ SAMPLE IN →

$\frac{M_T}{M_F}$ SAMPLE OUT →

% DETECTION

$\frac{M_T}{M_F}$ IN ARBITRARY UNITS
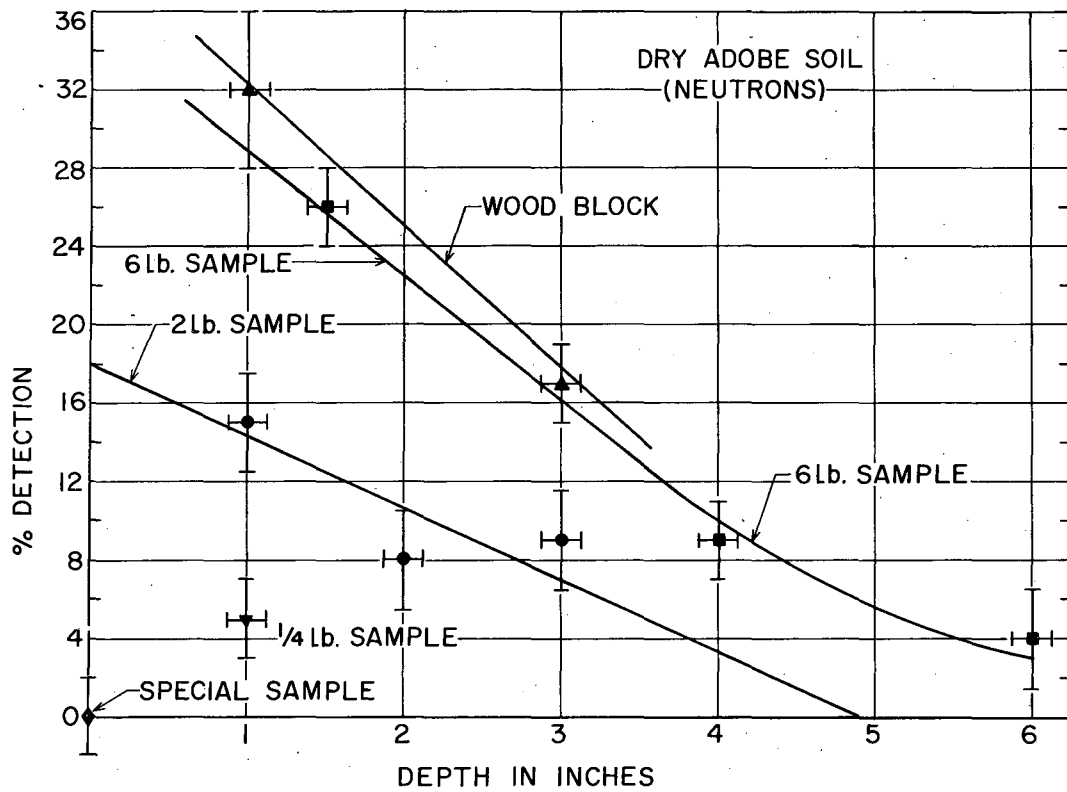
DISTANCE FROM EARTH TO COUNTER & SOURCE
IN INCHES
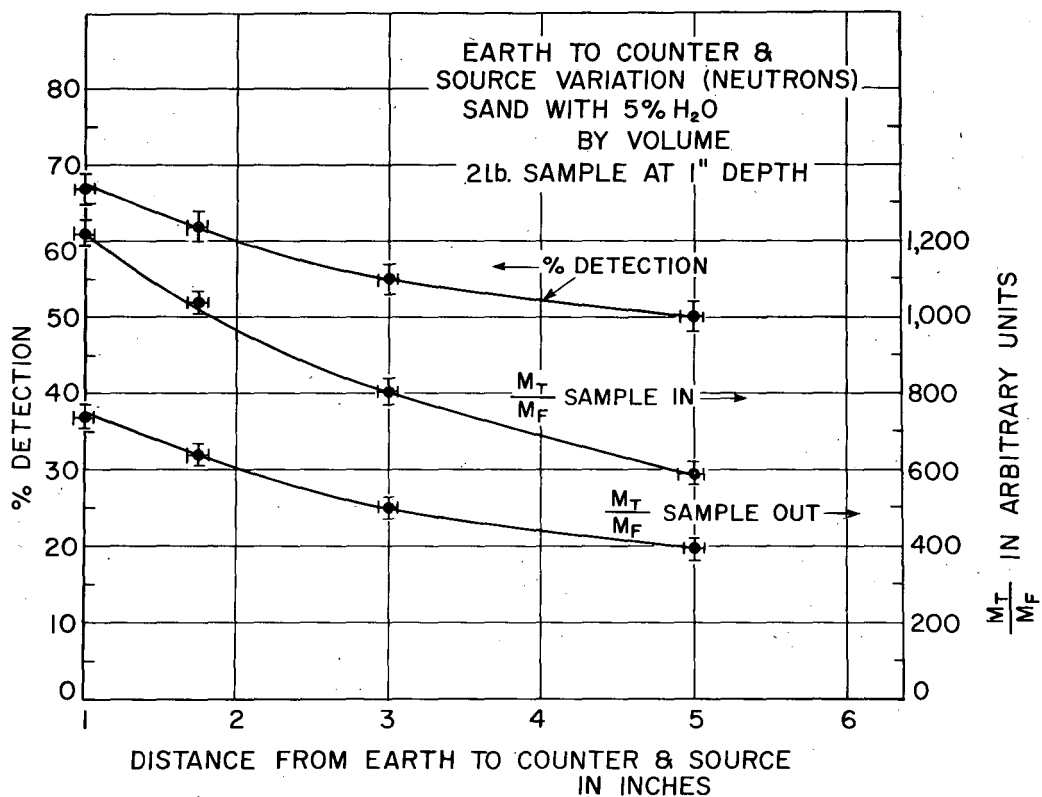
FIG. 12

MU-8822

Fig. 12. Percent detection vs distance from counter and source
to earth.

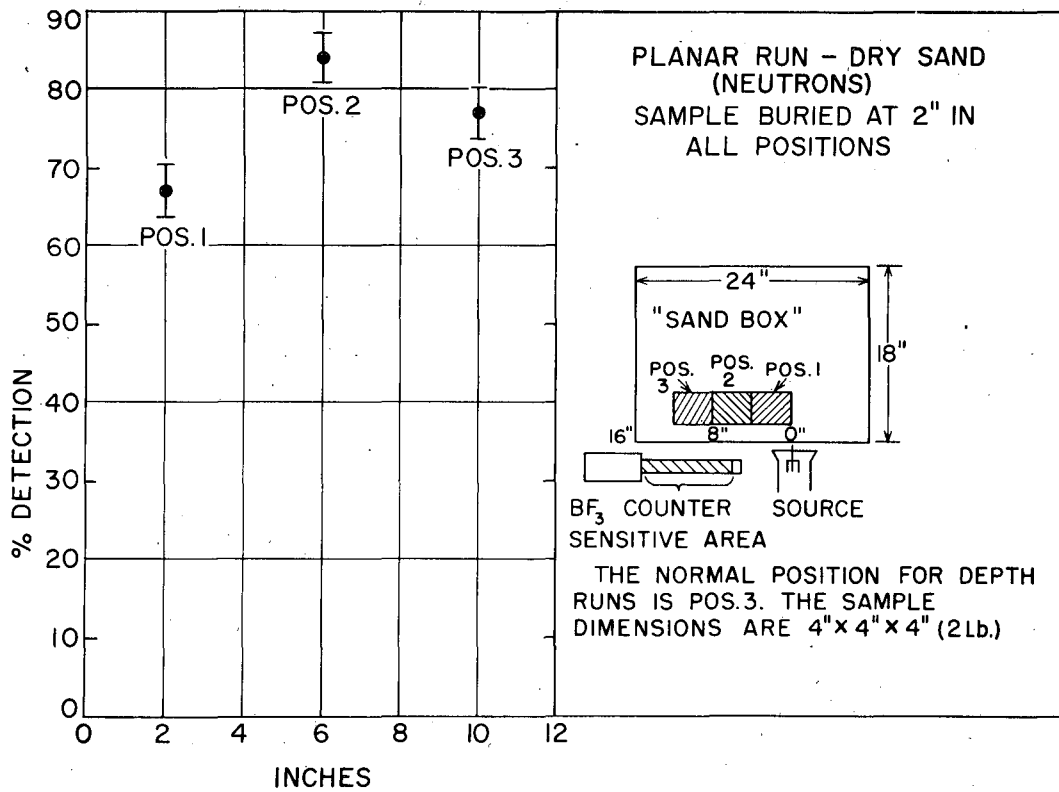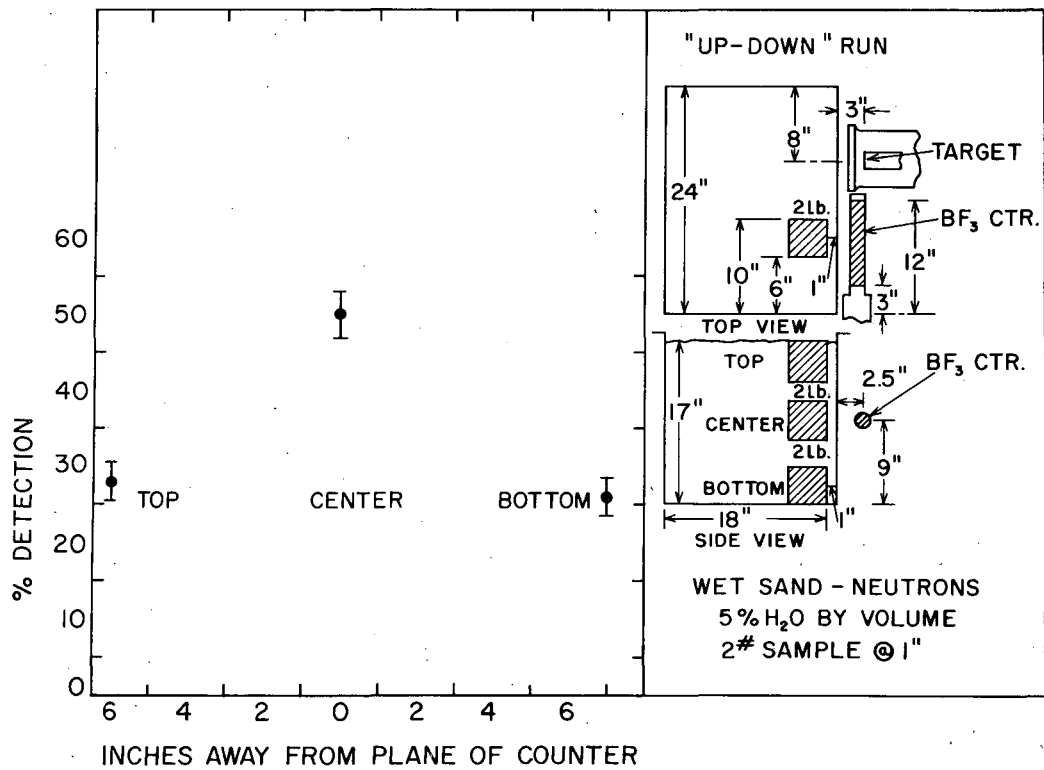Fig. 13. Percent detection vs sample position (constant depth).

Fig. 14. Percent detection vs sample position (constant depth).

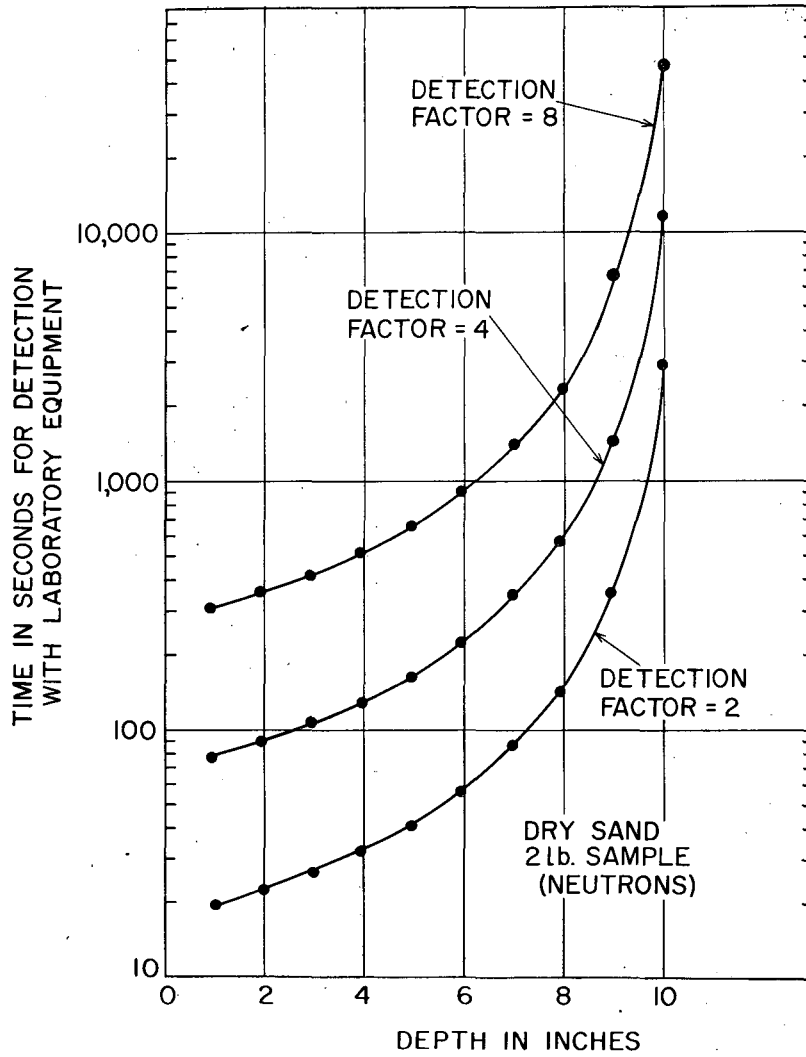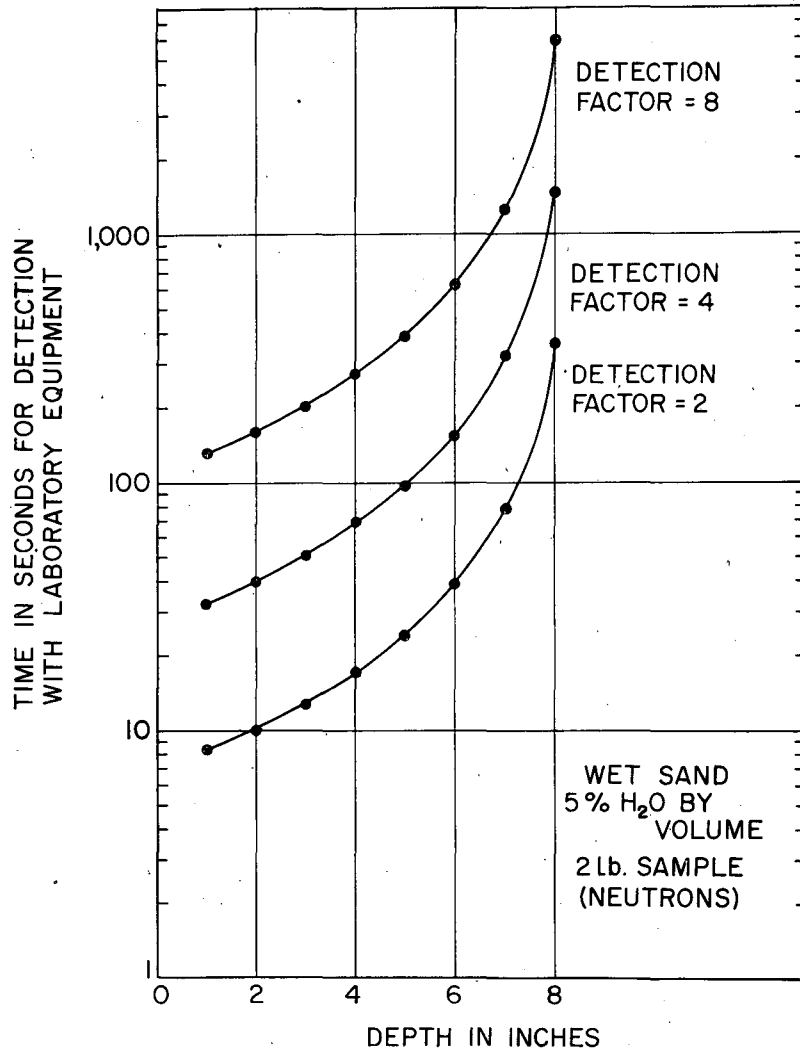Fig. 15. Time vs depth and detection factor for dry sand.

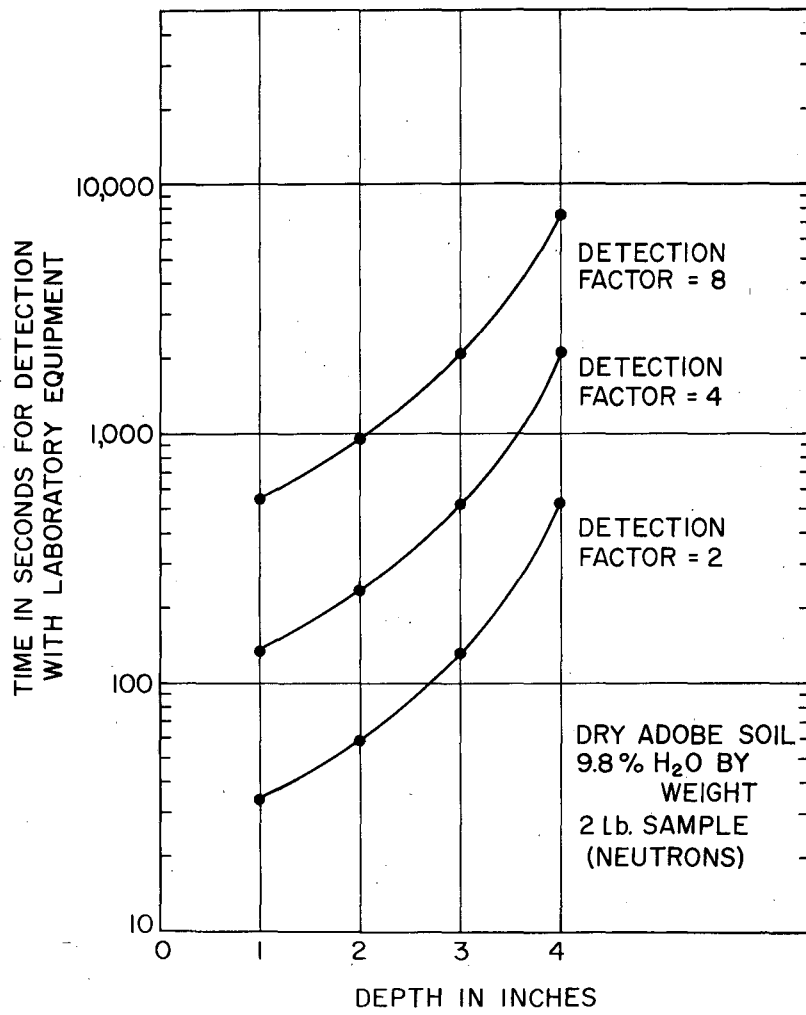Fig. 16. Time vs depth and detection factor for wet sand.

DEPTH IN INCHES

FIG. 17

MU-8781

Fig. 17. Time vs depth and detection factor for adobe soil.

DETECTION BY DELAYED-CAPTURE GAMMA RAYS

The geometry used for the detection of buried explosives by delayed-capture γ-rays is shown in Figs. 18 and 19. A sodium iodide crystal attached to a photomultiplier tube is used to detect the γ-rays emitted from the soil or sand under observation. A paraffin-moderated BF_3 neutron counter is used to monitor the neutron flux from the machine and is placed approximately 3 ft. from the neutron source (the same position as in the delayed-neutron method). The BF_3 counter was calibrated by placing a standard PoBe neutron source at the target position of the pulsed neutron source.

The γ-ray counter requires a lead house around it on all sides (except that facing the sandbox) in order to reduce background. The γ-counter signals are fed through a special shaping circuit and cathode follower to the gated scalers. The gating sequence for the scalers is shown in Fig. 6 and is identical to that used for the thermal-neutron method. Appendix II describes in detail the counter setup.

The method for determining the detection ratios follows the same steps as the method for delayed thermal neutrons. The neutron source is turned on and the net number of γ-ray counts vs the net number of counts from the neutron monitor is compared in a ratio of M_γ/M_n with sample in to M_γ/M_n with sample out, where M_γ is γ-ray count and M_n neutron monitor count.* These data are plotted in Figs. 20, 21, and 22.

With the use of a scintillator, such as NaI, it is possible to observe the energy as well as detect the presence of a γ-ray, since the amplitude of the output pulse of the photomultiplier is proportional to the γ-ray energy. With the process of detection by delayed thermal neutrons, the energy of the neutrons, being thermal, is essentially a constant and the neutron-detector counter detects only the presence of thermal neutrons and not their "energy".

A pulse-height analyzer is placed between the γ-ray detector and the counters in order to observe γ/n** ratios (both with sample in and sample out) vs energy (pulse height), and detection ratios vs energy. These data are plotted in Figs. 28, 29, 30, and 31 for wet sand and adobe soil. A search was made for a unique γ-ray line resulting from one of the capture reactions in the explosive, but no useful ones were found. The above-mentioned curves indicate that the detection ratio showed some variation with energy, but it was not helpful, because the peaks that occur at high energy are based on γ/n ratios that are, in some cases, less than the values at lower energy by a factor of about 10^2 (Figs. 29 and 31). This means that the γ-counting rate is down by a factor of 10^2 and it would cost this much time if the rest of the spectrum were discriminated out by a pulse-height analyzer for the relatively small gain in detection ratio. In other words, the integral γ/n values and resulting detection ratios described in Figs. 20, 21, and 22 are too close to these peak values to merit the sacrifice in counting rate.

---

*M_γ/M_n is the same as M_T/M_F for thermal-neutron method.

**$\gamma/n = M_\gamma/M_n$.

Detectors: Effect of Crystal Size

The efficiency of a given size NaI crystal decreases as the energy of the γ-rays increases. For detection of the delayed-capture γ-rays at lower energies, a cylindrical crystal 1.5 in. in diameter and 1.0 in long was sufficient. In order to observe the higher-energy γ-rays with practical counting rates, however, we used NaI crystal 3.5 by 3 in.

The curve for percent detection vs depth for dry sand (Fig. 20) was taken with this large crystal in order to determine if the detection ratios would be higher than with the 1.5-in. crystal. The detection ratios were the same in both cases. The count rate from the large crystal was much higher, however, because it would "look at" a larger area of soil and be more efficient at the same time. The data for the searching time and percent detection in dry sand (Figs. 20 and 25) are given for the 3.5-in. crystal. The remainder of the data were taken with the 1.5-in. crystal.

All calculations on scaling laws and those by which the scanning-time curves (Figs. 25, 26, and 27) were found are exactly the same as mentioned in the section on delayed-thermal-neutron detection.

The geometry considerations for the γ-ray counter are somewhat different from those for the neutron counter. In the neutron counter the sensitive volume is a cylinder about 8 in. long and 1.5 in. in diameter, but for the γ-ray counter, it is a piece of NaI 1.5 in. in diameter and 1 in. long. Obviously the γ-ray setup can "see" a much smaller area than an equivalent BF_3 counter (compare Figs. 13 and 24). The area seen by the 1.5-in. NaI crystal is of the order of 0.15 ft.^{2} It becomes apparent, therefore, that from two to three NaI counters are needed per one BF_3 counter.

Special Experiments

When this project was undertaken one of the possibilities discussed was the detection of a unique γ-ray from nitrogen resulting from the N^{14} (n, γ) N^{15} reaction. This reaction has predominant γ-rays at 10.8, 7.4, 6.3, 5.6, 5.3, and 4.5 Mev. As mentioned above, to efficiently see these high-energy γ-rays we used a large NaI crystal (3.5 in. by 3 in.). Any effect due to this reaction was undetectable with our equipment for the type of geometry and for the neutron fluxes encountered. The N^{14} (n, γ) N^{15} reaction does not appear to be a practical means of detection of buried mines.

It was suggested that the γ-rays resulting from neutron capture in mercury might be investigated, as many mines have mercury fulminate detonators. The cross section for neutron capture in Hg is rather high (380 barns). A 1-gram sample of pure mercury was fastened to the standard 2-lb sample of MHE and runs were taken with the sample only and then with the sample + 1 gram of Hg. No change in detection ratio was produced by the presence of the mercury at any γ-energy.

In order to be sure that the γ-rays we detected were truly due mainly to the hydrogen present we attempted to detect the presence of the following things: (a) aluminum (no effect), (b) liquid nitrogen (no effect), (c) carbon (no effect), (d) CO_2 in the form of dry ice (no effect). All the samples were about 3 by 3 by 6 in. and were placed from 1 to 2 in. deep in dry sand.

A series of runs in dry sand with the 2-lb sample at 2 in. was taken with a 1-in.-thick lithium hydride "filter" between the box and the γ-ray counter. Lithium has about a 7.5% abundance of Li^6, which has a thermal neutron cross section of about 900 barns. This is sufficient to attenuate (or absorb) all thermal neutrons before they strike the crystal. The capture reaction in Li^6 gives short-range charged particles, which cannot enter the crystal. The γ-rays are only slightly attenuated by this "filter". The detection ratios as well as the γ/n ratios indicated that the NaI was counting γ-rays and not thermal neutrons.

The d-d reaction, used for all experiments so far described, yields 2.8-Mev neutrons. A run was made with 1-Mev Li^7 (p, n) neutrons using the proton beam of the UCRL Van de Graaff. The results from 1-Mev neutrons coincided, within statistics, with the data taken with 2.8-Mev neutrons.

Method of Calibrating the Gamma-ray Counter

Because the γ-ray counter is energy-sensitive, it is important to maintain its calibration of energy vs pulse height. Every morning and night a calibration run was made to be sure that the equipment was not drifting. A standard PoBe source was placed in front of the γ-ray counter and a pulse-height analyzer run was made on the γ-rays from this source. If the energy peaks coincided for both the morning and evening runs the system had not drifted.

The calibration curve is plotted in terms of counts vs base-line voltage of the pulse-height analyzer with window width constant.

CONCLUSIONS

Gamma-ray Method vs Thermal-Neutron Method

The most important comparison in relating the two methods is that of percentage detection $[(DR - 1) \times 100]$. The following table will most adequately demonstrate the comparison. In the column marked "Best", the * indicates a point where one system detects and the other does not. We arbitrarily chose 10% detection points as the lowest useful ones, and gave depths for the best system at the 10% point. In all but two cases, the neutron method is superior.

Another major disadvantage in the use of the γ method is the complication that attends the use of sodium iodide scintillation detectors. The rapid variation of counting rate with pulse height would require exceptionally well-regulated power supplies and a much higher order of precision in the counting equipment. In addition, photomultipliers and the detecting crystals are both very fragile items. It would involve a large effort to engineer these items to field suitability. In principle, a large array of γ-ray counters could probably give higher counting rates than an equivalent array of neutron counters (for given source intensity). However, it seems apparent that the neutron method, with practical sources, will give counting rates such that the searching rate will not be limited thereby. It will be limited by practical vehicular speeds and operator abilities.

General

The ultimate aim, obviously, is to produce a field machine that will detect actual mines. The data in this report show that mines of sizes used today can in some cases be detected by this method. The signals on which the system works are not large. They are comparable with the best of other mine-detection methods in signal-to-noise ratio. The scheme will work in sand where other methods are said to fail completely, and is not too sensitive to small water contant in the soil being searched.

The translation of the laboratory equipment discussed in this report into a practical field instrument however, will involve many problems. Among these are the design of a suitable pulsed neutron source, the design of suitable electronics and display devices, and the design of an adequate platform to keep the equipment at a fixed small distance from the surface of the soil being searched. It must be emphasized that in total complication this device will be comparable with a small radar, and will require very well-trained personnel for operation.

If it is decided that there is sufficient need to warrant further exploration of this problem, it is recommended that a competent nuclear engineering firm be engaged to develop a suitable neutron source. In parallel with this, a group should be given the problem of translating the counter signals into data that an operator might use. Particular emphasis must be placed on the stability of every component, as it is necessary to make precise measurements on the signals (see Appendix II, Table II). In general, nuclear counting equipment is far more sensitive to variation in supply voltages, amplifier gains, circuit biases, etc., than radio or radar equipment.

But we believe that with sufficient attention to detail, an operable mine-detection device can be constructed utilizing the principles outlined in this report.

Table I

Table of Comparisons
% Detection

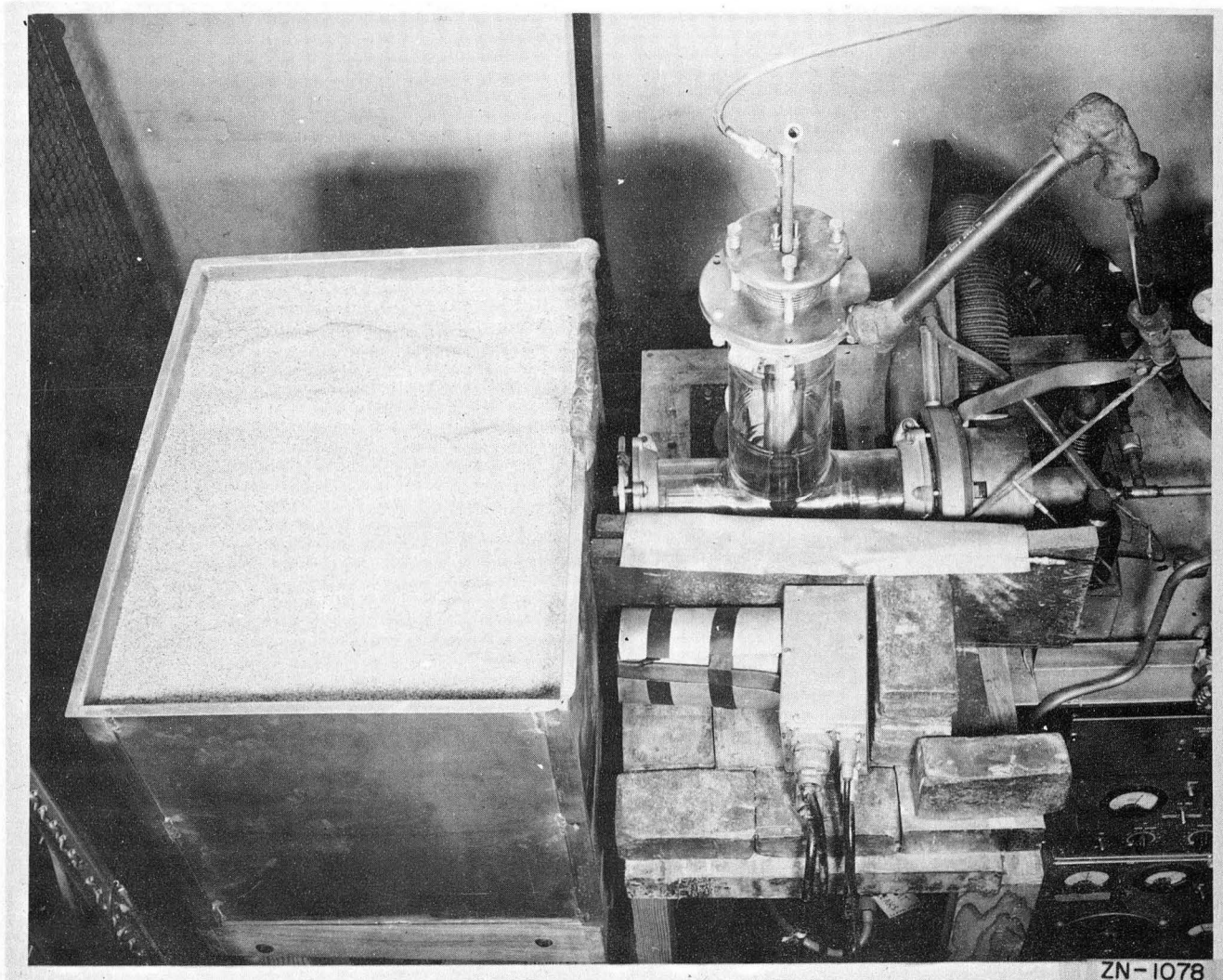| Sample	"Soil"	Depth (in.)	γ (%)	n (%)	Best
2 lb.	Dry sand	2	35	66	n
		5	12.5	43	n
		9 1/4	---	10	n*
6 lb.	Dry sand	2	~130	173	n
		5	51	96	n
		11 3/4	---	10	n*
2 lb.	Wet sand	2	29	57	n
		5	14	32	n
		7 3/4	---	10	n*
6 lb.	Wet sand	2	130	90	γ
		5	35	48	n
		10	10	10	same
2 lb.	Adobe	1	13	14.5	n
		2	10	10.5	n
6 lb.	Adobe	1	18	29	n
		2	12	22	n
		4	8	10	n

Fig. 18. Gamma-ray counter orientation. Showing soil box
(left), neutron source (rear center). Gamma-ray detector
counter (center foreground) is shown with lead-brick shield-
ing partly removed.

γ-RAY EXPERIMENTAL GEOMETRY
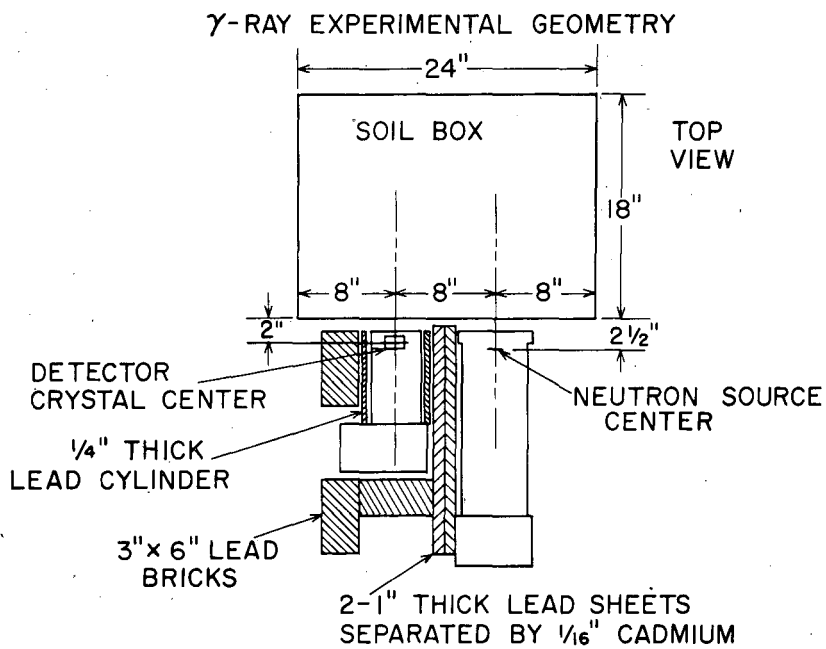
NOTE: 2" LEAD ABOVE AND BELOW
      COUNTER NOT SHOWN

FIG. 19

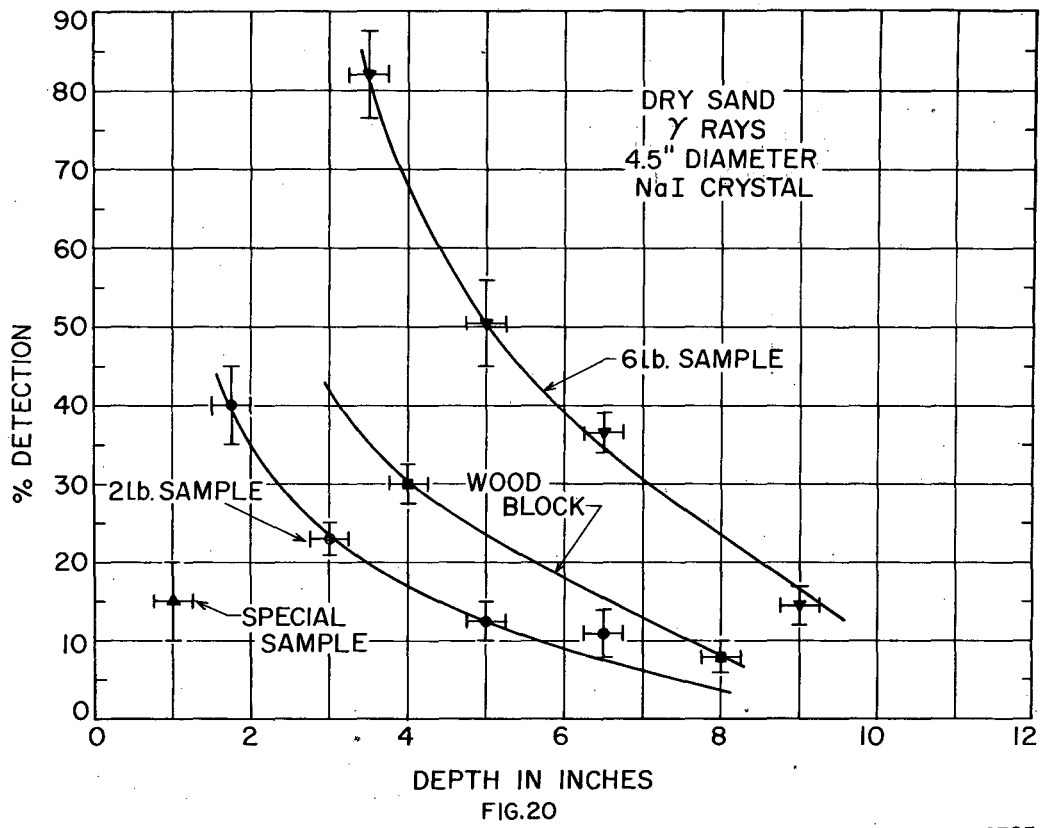MU-8782

Fig. 19. Dimensions of gamma counter geometry (laboratory
    arrangement).

Fig. 20. Percent detection vs depth for dry sand.
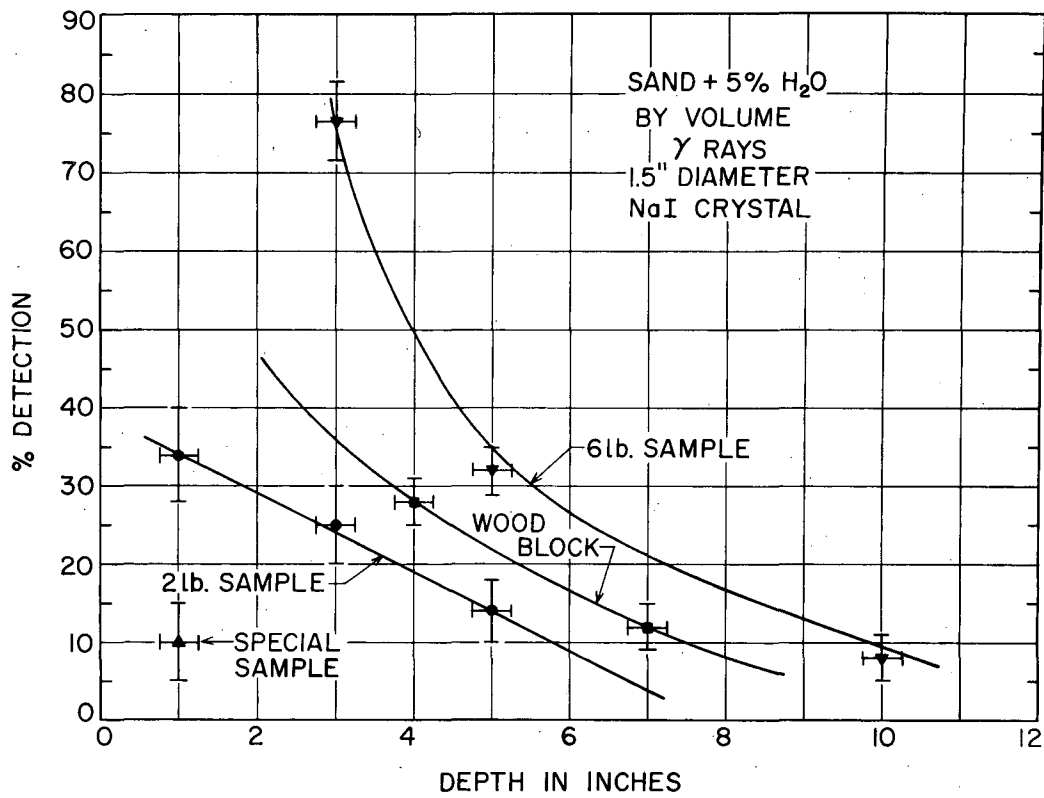
Fig. 21.   Percent detection vs depth for wet sand.
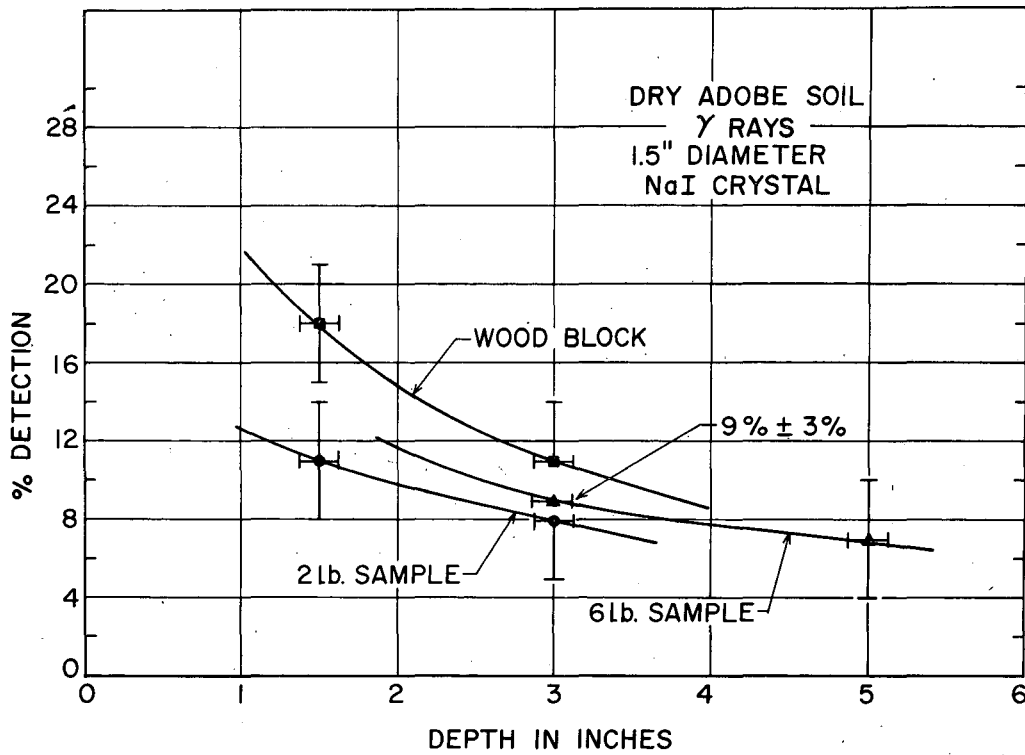
Fig. 22. Percent detection vs depth for dry adobe soil.
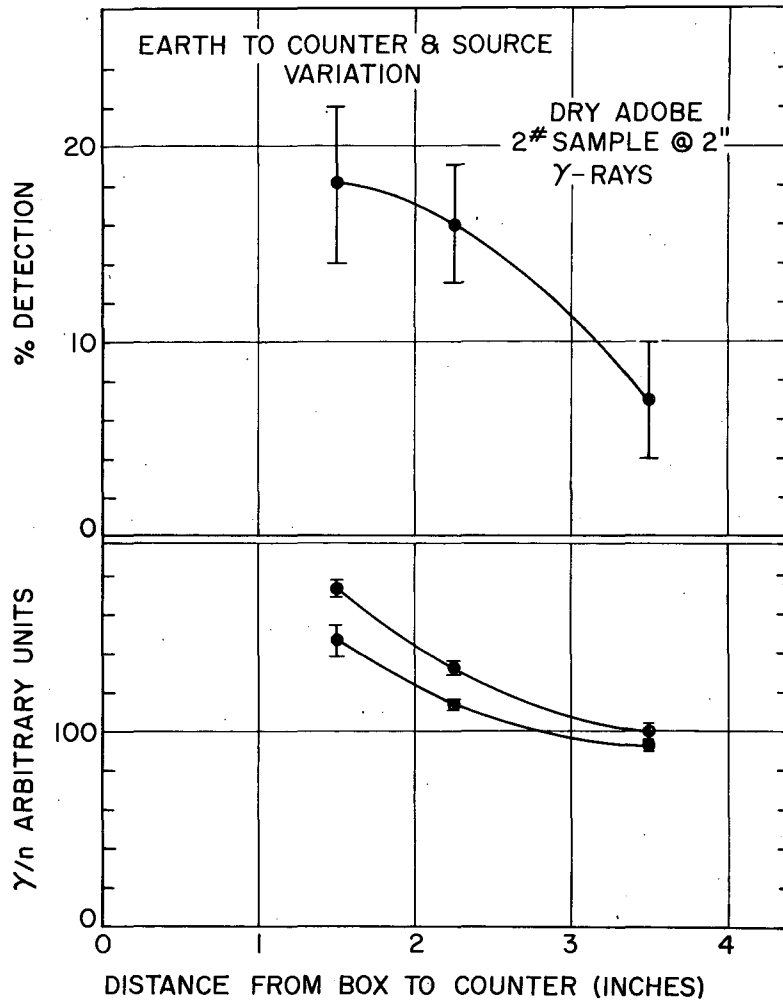
Fig. 23. Percent detection vs distance from counter and source
    to earth.
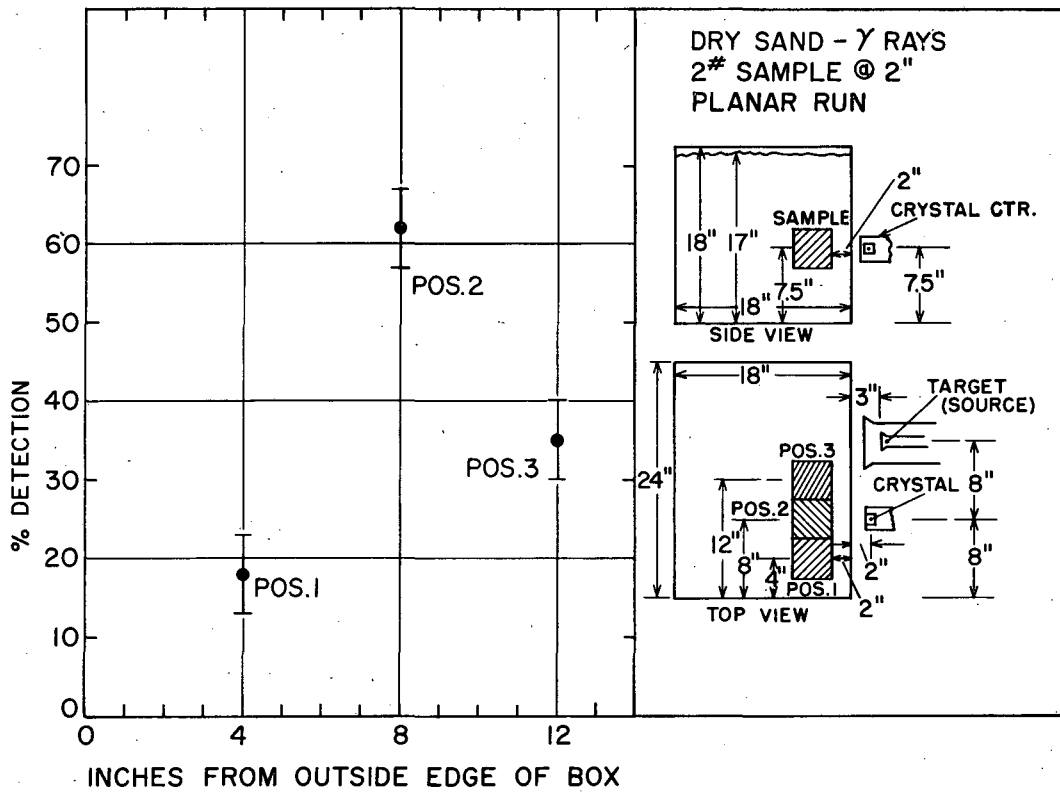
Fig. 24. Percent detection vs sample position (constant depth).
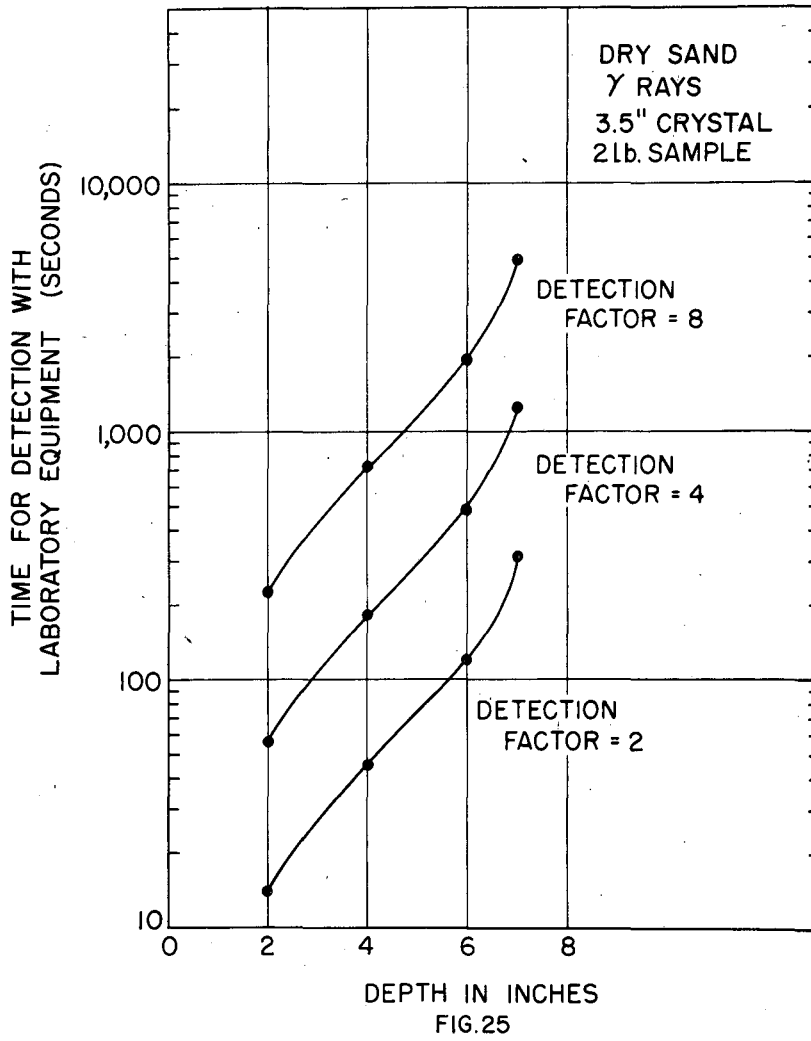
MU-8787

Fig. 25. Time vs depth and detection factor for dry sand.
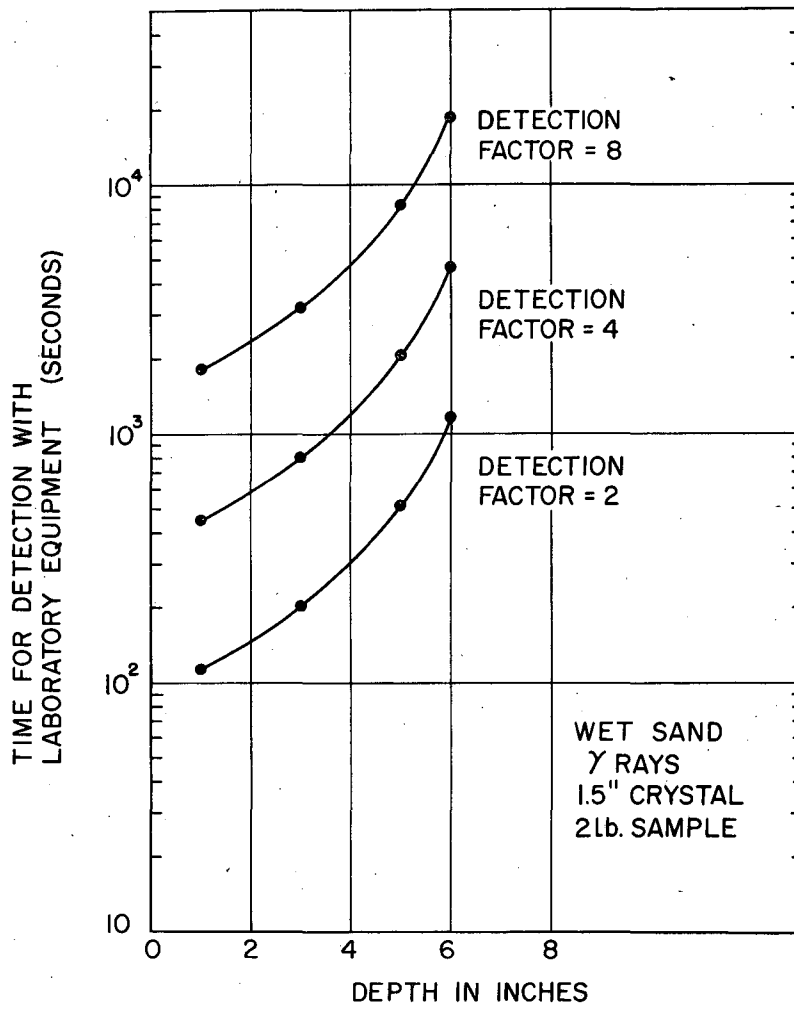
Fig. 26. Time vs depth and detection factor for wet sand.
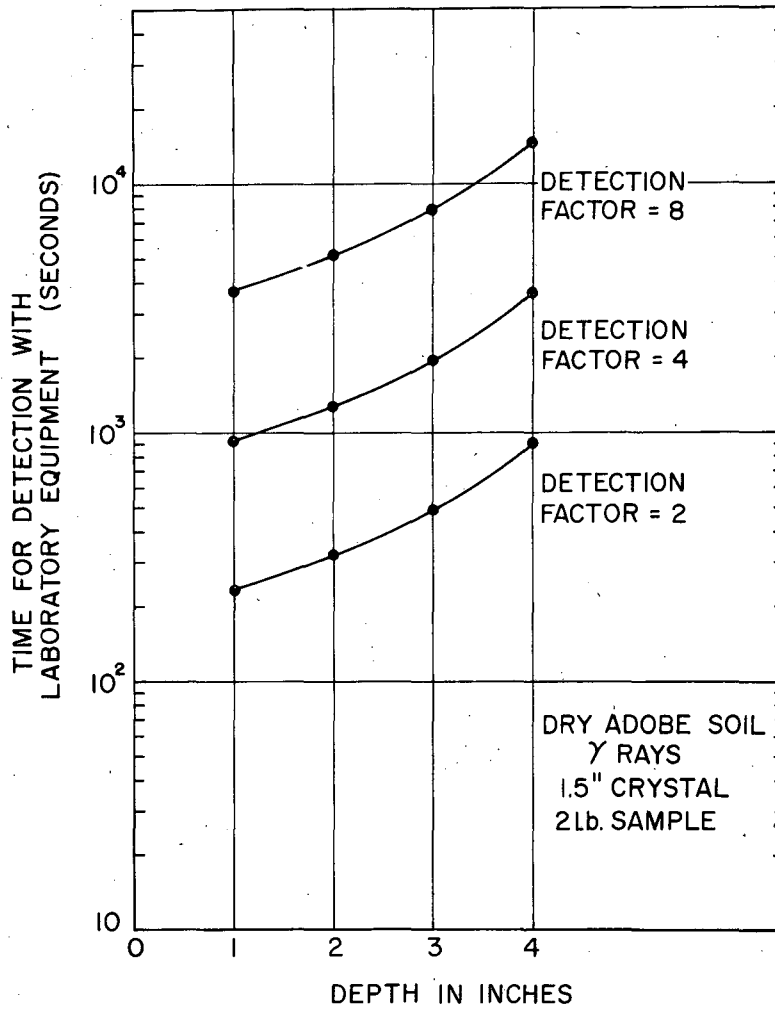
Fig. 27. Time vs depth and detection factor for dry adobe soil.
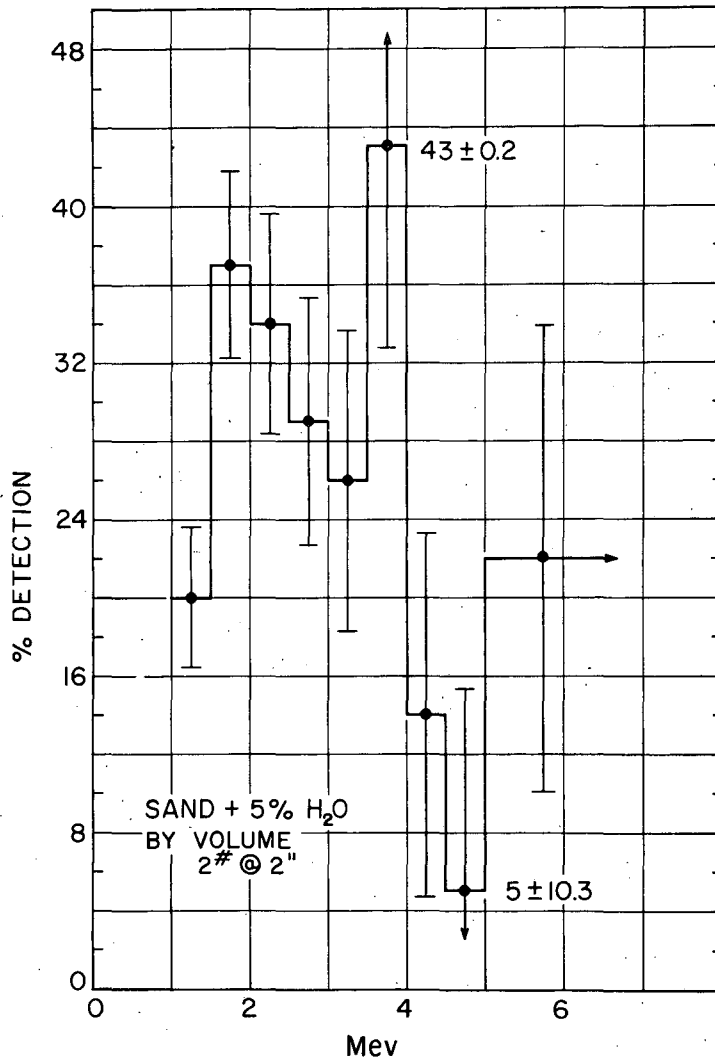
Fig. 28. Percent detection vs energy for wet sand.
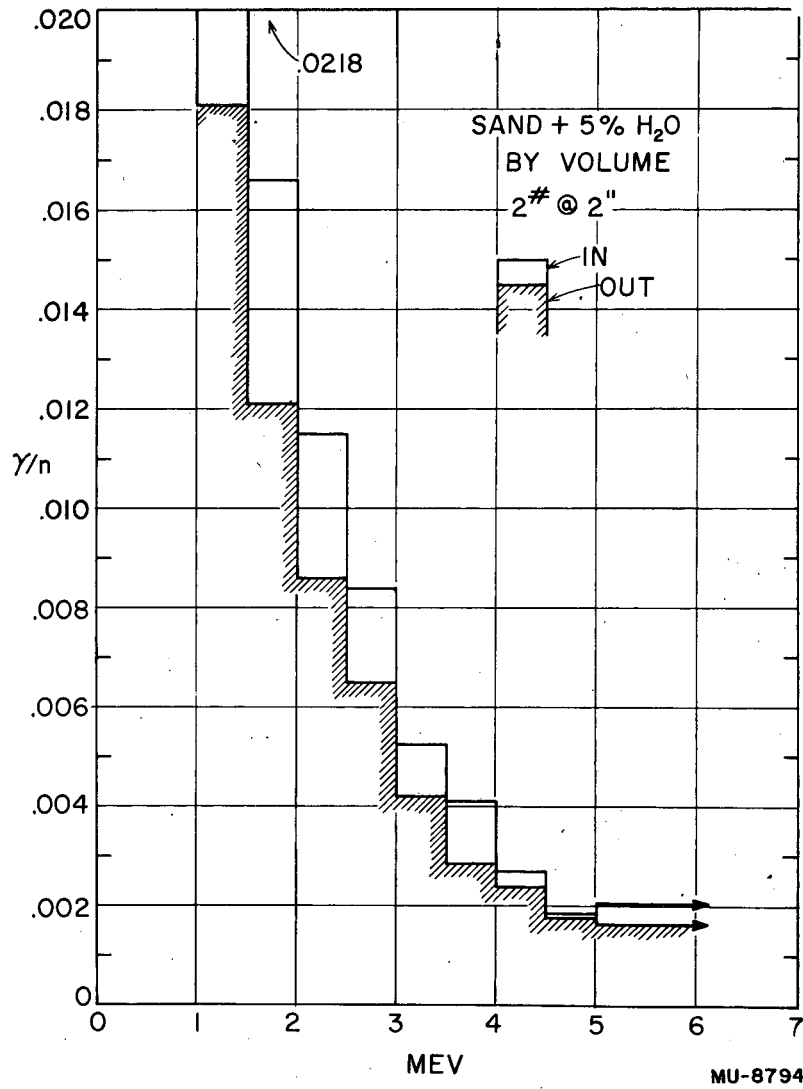
Fig. 29.   Gamma-to-neutron ratios vs energy for wet sand.

Fig. 30.   Percent detection vs energy for dry adobe soil.

Fig. 31. Gamma-to-neutron ratios vs energy for dry adobe soil.

APPENDICES

I.   (d, d) Neutron Source

The pulsed neutron source (Fig. 32) provides neutrons of about 2.8 Mev energy. It produces of the order of 10^5 neutrons per 200 μsec pulse at a repetition rate of sixty pulses per second.

It consists of a vacuum system, a "Pig" (Phillips Ion Gauge) type ion source, a deuterium gas supply and palladium leak valve, a titanium deuteride target, a high-voltage dc power supply, electronics for operating the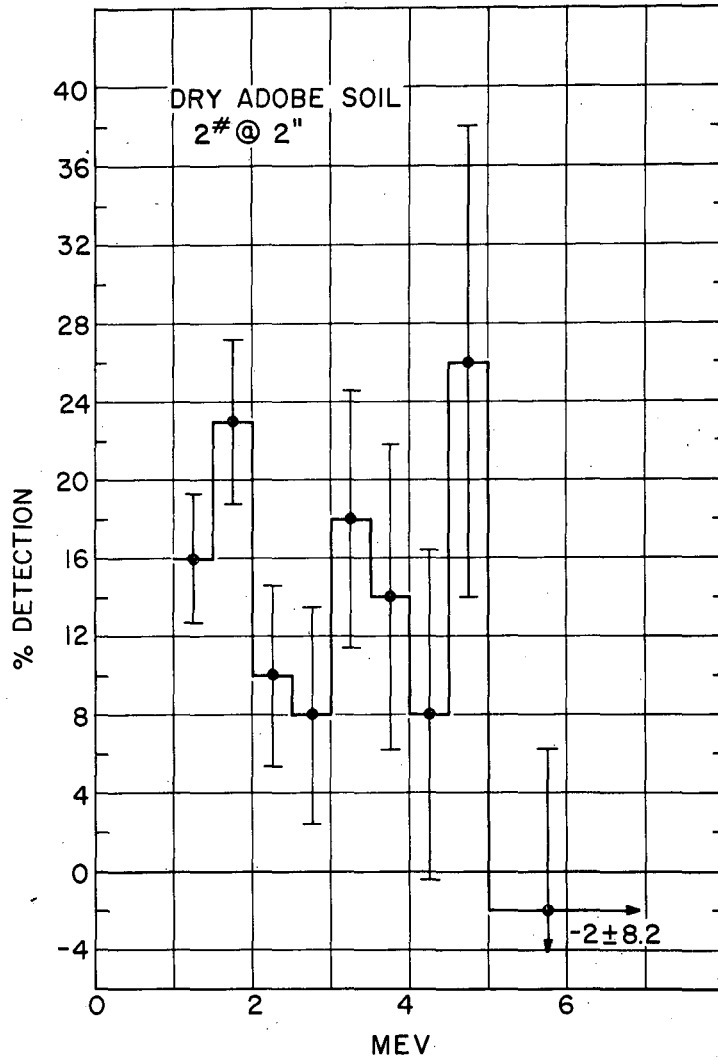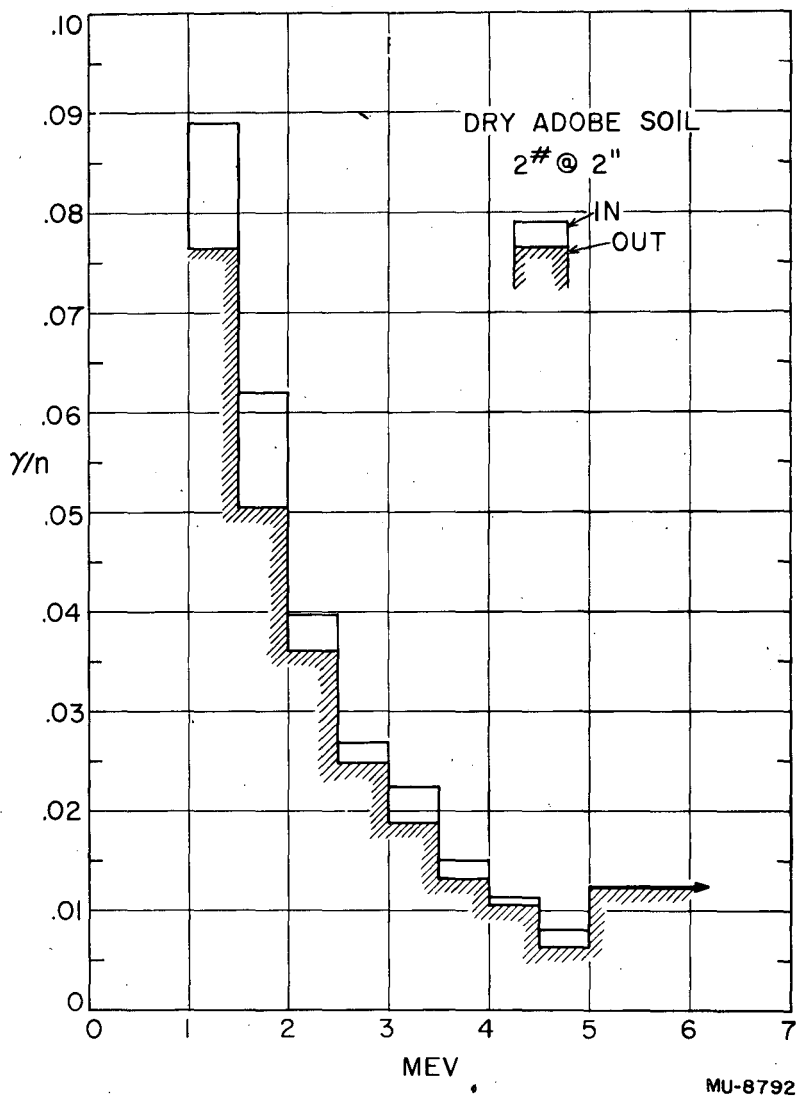 Pig, and various adapter plates, target holders, etc. The Pig ion source produces deuterons from the deuterium gas, which is admitted via the palladium leak. The positively charged deuterons are extracted from the Pig by the negatively charged probe electrode, are controlled by the focus electrode, and are accelerated in vacuum by the high-voltage dc supply, then strike a titanium deuteride target, producing neutrons by the (d, d) reaction.

Vacuum System

The vacuum system (Fig. 33) consists of a 3-inch water-cooled diffusion pump, made by Consolidated Vacuum Corp., backed by a CVM 3153 Kinney mechanical forepump. A liquid-nitrogen-cooled surface traps condensable materials, and a gate valve between trap chamber and high-vacuum chamber permits work to be done on the system without letting air into the diffusion pump. A valve manifold between the diffusion pump and forepump allows the latter to be used for rough-pumping the high-vacuum chamber and provides connections for leak detector or external roughing pump. It was found necessary to increase the diffusion-pump heater power in order to pump deuterium efficiently. This was accomplished by operating the diffusion-pump heater at 150 volts from a variac transformer, though the pump heater was designed for 115-volt operation. National Research Corporation Type 501 vacuum thermocouple gauges in the trap chamber and the valve manifold assist the operator during pumpdown and a Type V.G. 1A/2 ion-gauge tube in the high-vacuum chamber monitors the system pressure during operation. Power switches, ion-gauge and thermocouple-gauge power supplies, and diffusion pump variac are mounted on standard rack panels on the front of the vacuum-system cabinet. This system produces a vacuum of about 5×10^{-5} mm Hg with normal operating gas flow from the ion source.

Pig Ion Source

The Pig ion source produces about one milliampere peak deuteron current during the pulse. It consists of a tubular anode of nonmagnetic stainless steel mounted axially between two grounded parallel aluminum cathodes in an axial magnetic field of about 1000 gauss (Fig. 34). The anode is supplied with 200-μsec pulses of about 1500 peak volts during which about 3 amp of ion current flows. Some of the ions produced are extracted through the exit aperture--an opening of 0.030 to 0.040 inch diameter--through one cathode. The ions are extracted by a high negative potential (30,000 volts with respect to ground) on a hollow probe electrode behind the exit aperture, pass through the probe, a focus electrode, and the target electrode before impinging upon the target. The anode, cathode, and probe electrode are contained within a stainless steel arc chamber about 1-5/8 inch in diameter and 5 inches long.

Through one end of this chamber pass the gas-admission tube and the anode
connection. On the other end is attached an iron flange 8-1/4 inches in di-
ameter and 0.5 inch thick, which supports the arc chamber itself and the
focus-electrode mounting insulators as well as acting as a pole piece for the
Pig magnet. The magnet coil is wound on an iron and brass bobbin which
slips over the arc chamber, the iron end forming the other pole piece. The
coil has 6,000 turns, operates at about 1.3 amp, and is cooled by a small
air blower. The focus electrode operates at about 28,000 volts negative
with respect to ground.

Mechanism of the Discharge*

Although many are familiar with the basic mechanism of the Penning
discharge, it is reviewed here briefly. Consider the geometry of Fig. 34
with a deuterium pressure in the arc chamber of the order of 20 μ, a mag-
netic field in the range of a few hundred gauss, and a positive potential in
the range of a few hundred volts existing between the anode and cathodes.

If an electron is released from either cathode it will be accelerated
into the anode, its radial motion constrained by the magnetic field. The
electron will coast through the field-free region in the anode, losing some
energy to the gas, and leave the anode at the other end with somewhat less
energy than it gained in the initial acceleration. But it will be reflected by
the electric field, re-enter the anode and continue its axial oscillation. In
these oscillations it will sooner or later make several ion pairs, losing en-
ergy in the process. Since the energy lost in ionizing is of the order of 35
volts, and the initial energy of the electron is several hundred volts, approx-
imately ten ions will appear inside the anode before the initial electron is
below ionization energies. These ions are also constrained by the field,
their principal motion therefore being axial. Eventually, they will come
to one end of the anode, where they will be accelerated into the correspond-
ing cathode.

For deuterons of a few hundred volts incident on an aluminum oxide
surface, there is a finite probability that a secondary electron will be released.
Such electrons will be accelerated into the anode region to continue the ion-
izing process. Although we lack good data on the magnitude of the ratio N
of deuterons to secondary electrons for aluminum oxide, it seems reasonable
to assume that it will lie between 5 and 10 in our case. If the number of ions
produced by the first electron is greater than N, the discharge will increase
in intensity until limited by other mechanisms. This limit is normally set
by an external series resistance in the anode circuit, which causes the anode
potential to fall as the discharge increases. Under this condition an equi-
librium will be reached between the number of secondary electrons produced
per ion and the number of ions produced per fast electron.

Pig Gas Supply and Palladium Leak Valve

Deuterium gas is supplied to the Pig from a 500-cc container filled
to about 5 psig (Fig. 35). This supply is sufficient for about 30 hours of
operation. Flow of gas is controlled by passing it inward, through the thin

---

*From James D. Gow and John S. Foster, Jr., A High-Intensity Pulsed
Ion Source, Rev. Sci. Instr. 24, 8, 606 August 1953.

walls of a palladium tube inside the gas container, the flow rate being a function of the temperature of the tube. The tube-wall thickness is about 0.005 inch. The palladium tube is surrounded by a heater within the gas tank which is a standard radio-type 50-ohm 50-watt wire-wound resistor. Electrical connection to the resistor is brought through the container end via a gastight bushing. The leak starts to open at 25 to 35 volts obtained from a variac. One end of the palladium tube is sealed shut and the other is hard soldered to the copper gas-outlet pipe that passes through the container end wall to a valve manifold and thence to the Pig. The valve manifold permits evacuation of the pipeline and admission of air for oxidizing the Pig cathodes. A Type 501 vacuum thermocouple gauge monitors the gas pressure in the line near the Pig. The normal operating pressure is 55 μ, as read with this type gauge. The pressure read with this gauge is about 3 times as high as the actual pressure because of the greater heat conductivity of deuterium than of the gases for which the gauge is normally calibrated.

Target

The target is made by melting titanium metal on tantalum foil in a vacuum and then reheating and slowly cooling it in a deuterium atmosphere. The titanium takes up about 450 cc (STP) of deuterium per gram under ideal conditions. Heating the target in vacuum drives off the gas, so it is necessary to keep the target cool while using it in the machine.

High-Voltage dc Supply

The high-voltage target supply (Fig. 36) is of the Cockcroft-Walton type, and produces 90 kilovolts dc from 110-volt 60-cycle input power. The output current is limited by 100 megohms of series resistance. The output charges about 11 feet of R.G. -17/U cable, which carries the power to the target electrode and supplies about 300 $\mu\mu$f of capacity to stabilize the target voltage during the pulse. A 1,000-ohm resistor between cable and target electrode limits the breakdown current if sparking occurs from target electrode to ground. An interlock chain in the grounded safety screen around the equipment breaks the power-supply input power and drops an automatic grounding hook on the high-voltage lead if entry is attempted with power "on".

Pig Operating Electronics

The Pig operating electronics (Fig. 37) consists of a 0- to 2-kv positive dc supply capable of 50 ma, a hard tube pulser for 2,000-volt 3-amp 200-μsec pulses, a 60-cycle line synchronized trigger multivibrator, a 0- to 200-v dc supply at 1.5 amp, two 0- to 30-kv negative dc supplies at 1 ma, and various resistor-capacitor networks. The 0-2 kv 50 ma positive dc supply provides adjustable power to the Pig arc. This power is pulsed "on" for 200 μsec out of each 1/60 sec by the hard tube pulser and the pulses are sent to the Pig anode. The pulse wave form is stabilized by the arc-stabilizing network--a 100-ohm resistor and 0.005 μf capacitor in series from pig anode to cathode. The pulser is triggered by the trigger multivibrator. The 200-V 1.5 amp dc supply provides Pig magnet power, and the two 30-kv 1-ma supplies provide probe- and focus-electrode power. The probe and focus voltages are stabilized by 0.05 μf 30 kv capacitors at the electrode terminals. Resistors in series with these capacitors limit the discharge current if electrical breakdown occurs within the vacuum system. A 10%

voltage variation in any of the Pig power supplies is negligible so none are regulated. The 200 V 1.5 amp magnet supply is full-wave rectified and feeds a highly inductive load so no filtering is necessary.

Sixty-Cycle Trigger Multivibrator

The trigger multibivrator produces the main trigger pulse for all equipment used in this experiment. It consists of two pentode clipper amplifiers in cascade, a differentiating circuit and a 70 μsec one-shot multivibrator. A 3.1-volt signal is fed to the first clipper from the tube filament supply. The clippers have sufficient gain to provide a square pulse that triggers the multivibrator via a 10-μsec differentiating circuit within about 5 μsec of the phase zero of the 60-cycle line. This precision was desirable to prevent line transients from causing timing jitter, which might trigger the neutron source while a background-counter gate was still open. The gain is also desirable to permit synchronizing to a low-power audio oscillator for operating at repetition rates of other than 60 cycles.

Probe and Focus Supplies

These supplies are commercial Condenser Products Corporation P.S. 30 supplies. They are provided with external time-delay relays, voltage-control variace, and meters. Suitable interlock protection should be provided to disable these supplies when working within the screened area.

Notes on Pig Operation

The following notes on Pig operation are given for reference, as some difficulty may be encountered in getting a new Pig started. Once started the Pig is very reliable.

(a) Cathodes must be clean. They should be machined without any lubricant from pure aluminum.

(b) Cathodes should be oxidized. A highly oxidizing torch flame should be applied to their surfaces before assembly. Each morning the Pig should be operated on air for about 5 minutes.

(c) Application of probe electrode voltage helps start the Pig.

(d) The Pig wave form appears as a spike 1000 volts high (normal power supply voltage) followed by a rectangular tail about 400 volts high.
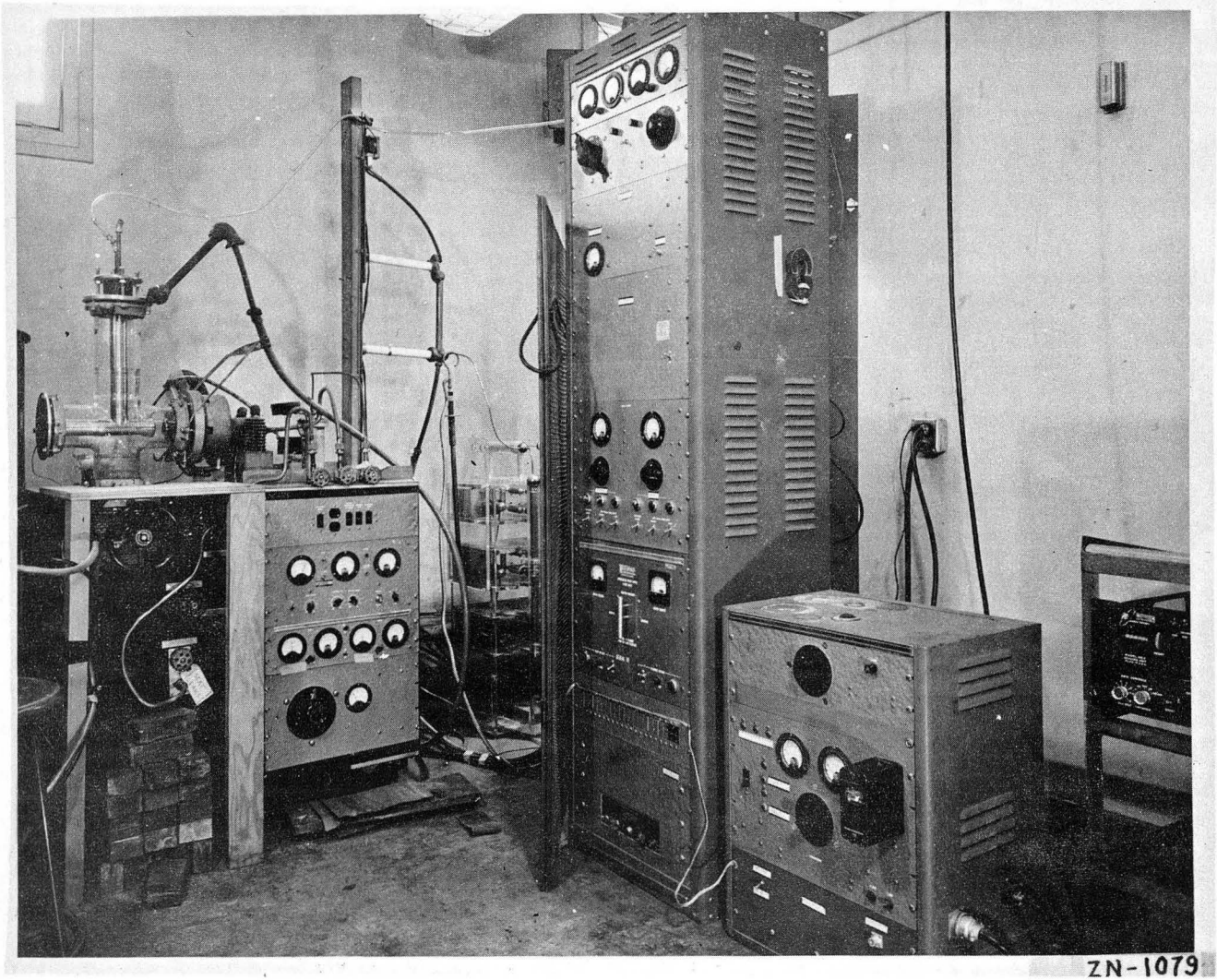
Fig. 32. Pulsed neutron source. Showing vacuum system and vacuum-measuring equipment (left), 90-kv power supply (rear center), two accelerator control racks (right).

VACUUM SYSTEM BLOCK DIAGRAM
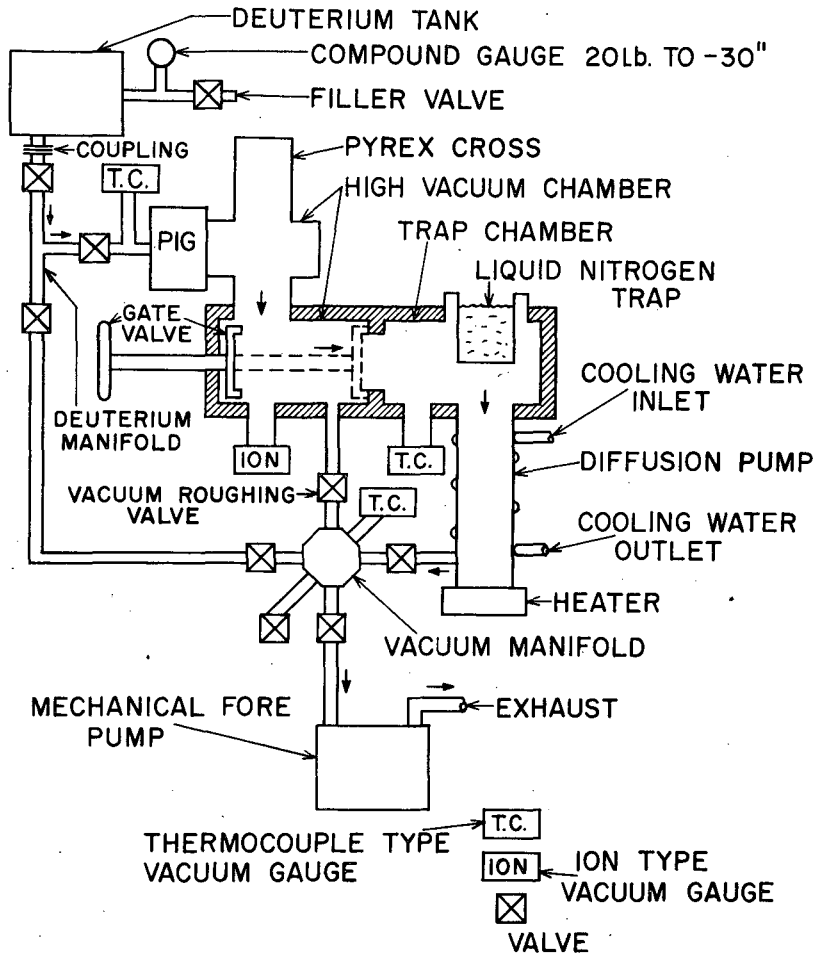
FIG. 33

MU-8824

Fig. 33. Diagram of vacuum system.

PIG

HIGH VOLTAGE FEED
THROUGH BUSHING

MAGNET COOLING AIR INLET

MAGNET COIL

GLASS VACUUM
CHAMBER

ALUMINUM
CATHODES

ANODE

GAS
ADMISSION
TUBE

ANODE
CONNECTION

ARC CHAMBER

MAGNET COIL
BOBBIN

TARGET
ELECTRODE

EXIT APERTURE

FOCUS ELECTRODE

PROBE ELECTRODE

FOCUS ELECTRODE MTG. INSULATORS

PIG ADAPTER RING
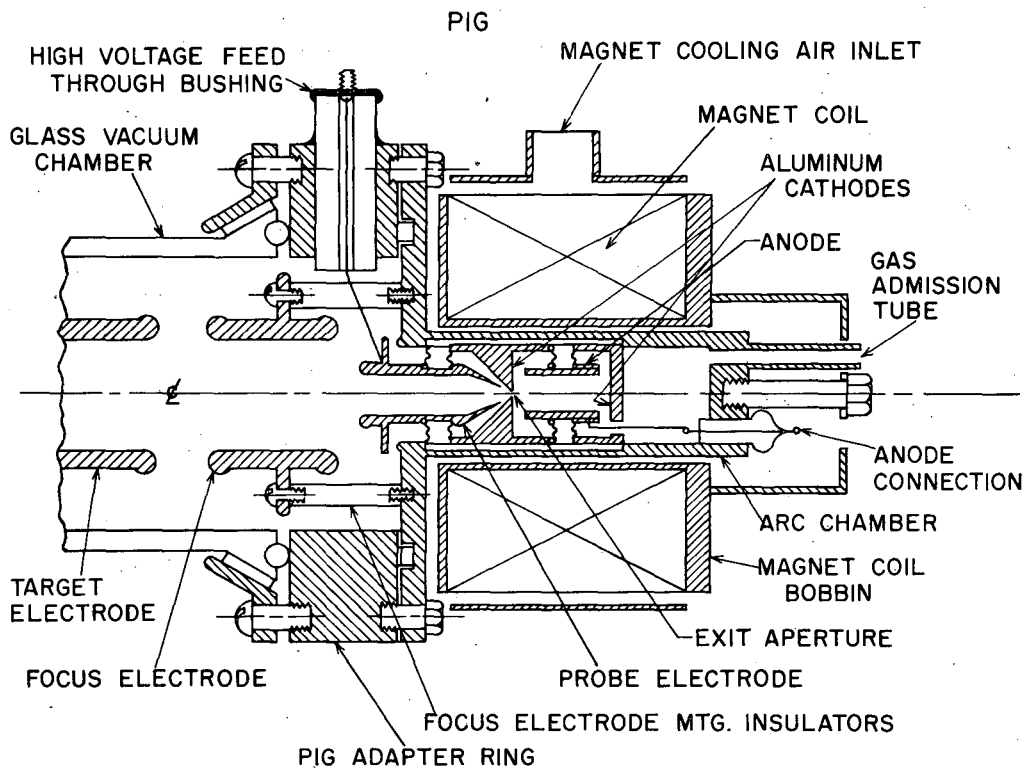
FIG.34

MU-8795

Fig. 34. Diagram of PIG ion source.

D$_2$ TANK AND PALLADIUM LEAK

DEUTERIUM OUTLET TO PIG

TANK FILLING
VALVE

GAS TIGHT
BUSHING

"O" RING
GASKET

50 Ω 50W
HEATER
RESISTOR
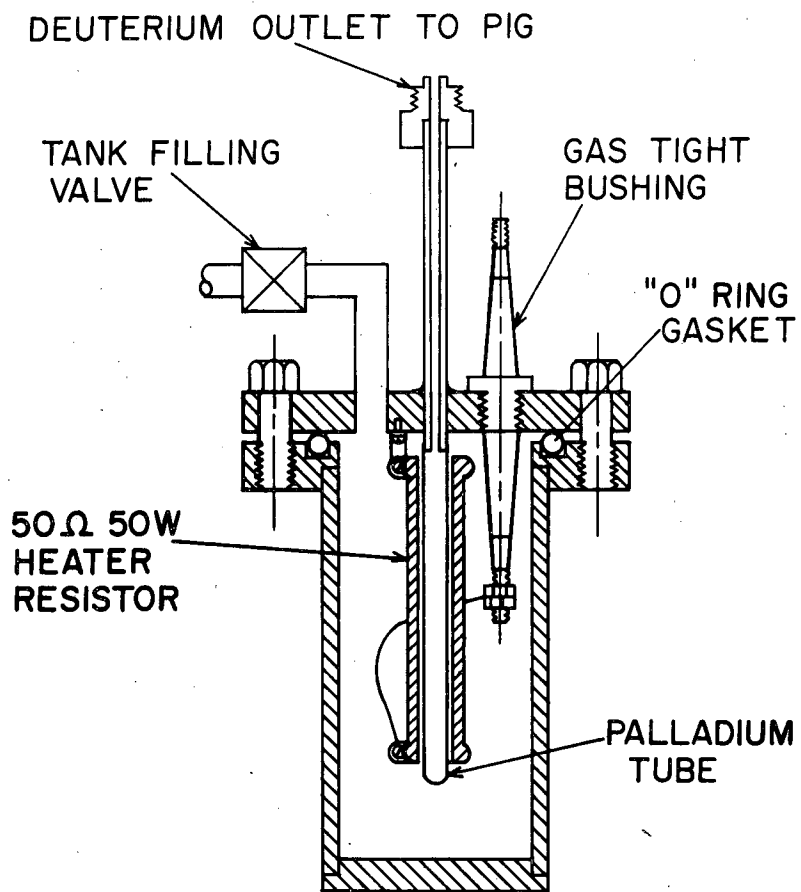
PALLADIUM
TUBE

FIG. 35

MU-8796

Fig. 35.   Diagram of palladium leak "valve".

90 KV POWER SUPPLY

HEINEMAN
AM-12

10 AMP   RE-1

110V 60~

RE-2
O.L.

(R)
INTERLOCK

(R)
INTERLOCK

(R)
STOP

(G)
START

RE-1

(R)

RE-1

RE-2

110V-10A
VARIAC

SOLENOID

11ft RG 17/U

SE-1   R-1 R-2 R-3   R-4

SE-2 ─ C-1   R-5

C-2 ─ SE-3

SE-4 ─ C-3   R-6

C-4 ─ SE-5

SE-6 ─ C-5   R-7

C-6 ─ 12 KV-.07A

R-8

110V - 7.4A

TO
TARGET
-90 KV

100μa F.S.
CALIBR.
0-100 KV

SURGE PROTECTOR
SUNCO CAT.#5130

0-500μa

C-1 THRU C-6 -.05μf 30KV
R-1,R-2 - 50 MEG 30W MVO
R-3 - 10K 200W
R-4 - 1K 200W
R-5, R-6 - 500 MEG 30W MVO
R-7 - 20K 1W

R-8 - 240K 1W
SE-1 THRU SE-6 5-200 CELL
RECTIFIER STACKS IN SERIES
USING FANSTEEL TYPE AD CELLS

FIG. 36

MU-8825

Fig. 36.   Diagram of 90-kv dc supply.

PULSED NEUTRON SOURCE BLOCK DIAGRAM

FIG.37

MU-8797

Fig. 37. Block diagram of accelerator electronics.

II. Counting Equipment

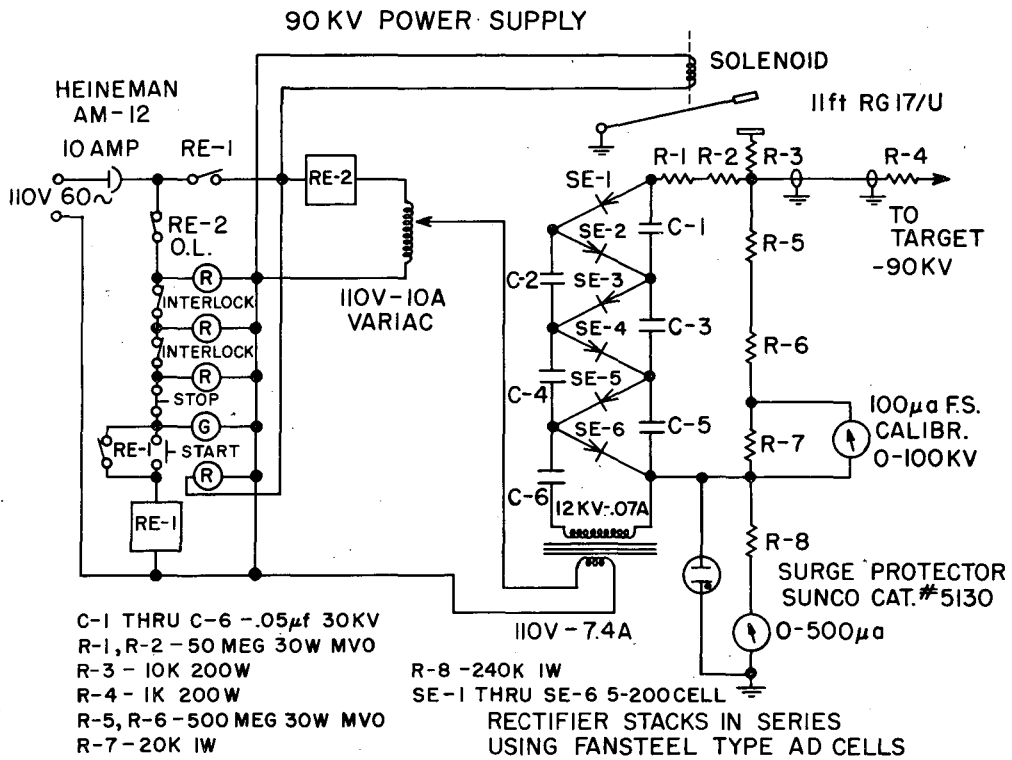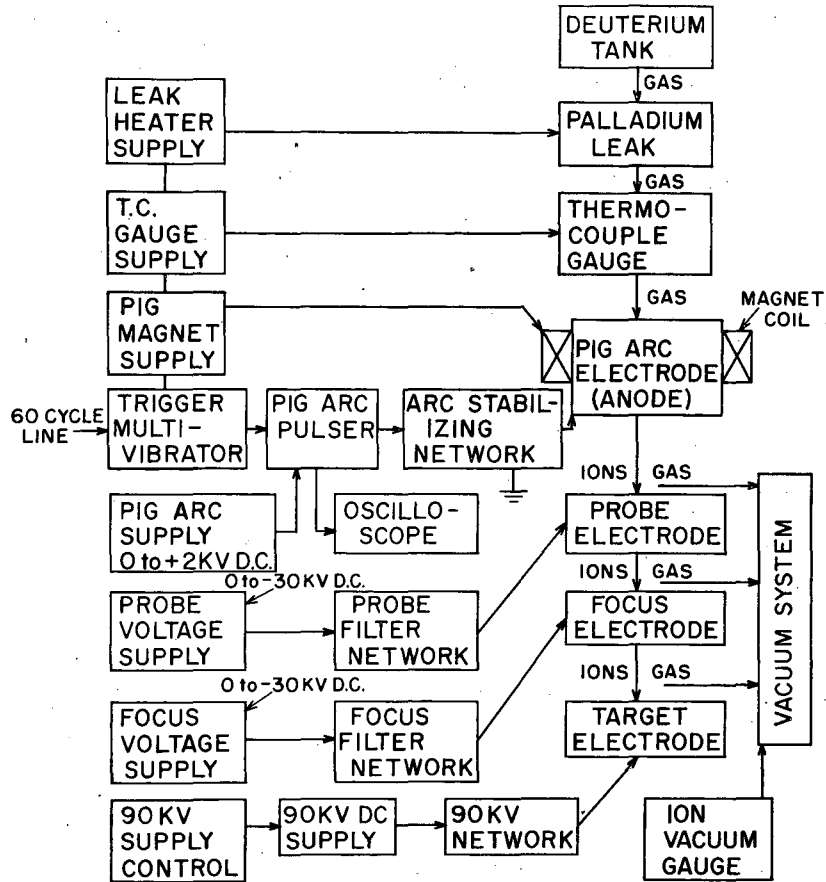The counting equipment (Fig. 38) consists of a neutron counter for monitoring the total neutron burst and either a slow-neutron counter or a γ-ray counter to act as a detector. The pulses from these counters are amplified in two "linear" amplifiers, sorted for size by discriminators and a pulse-height analyzer and totaled on scalers. The scalers are gated "on" at the proper times by enabling pulses from the tandem scaler-gating unit. The tandem scaler-gating unit is triggered by the trigger multivibrator that triggers the neutron source.

Neutron Counter

The neutron counters are of the BF_3 proportional gas type using gas enriched in B^{10}. These counters are of the geometry shown in Fig. 39 and use a 0.003-inch-diameter stainless steel center wire. They utilize the reaction $B^{10} + n \rightarrow Li^7 + \alpha$ to produce the necessary ions for counter operation. The cross section for this reaction drops rapidly with increased neutron energy, so it is necessary to surround the counter with a paraffin moderator when it is to be used as a fast-neutron monitor for measuring the total neutron yield of the source. The typical thickness of paraffin used is 1.5 inches. Signals from these counters are coupled into the signal cables to the linear amplifiers by means of cathode followers.

In the calibration of these counters with a source producing both neutrons and γ-rays, a plateau in the curve of count rate vs counter-supply voltage occurs typically between 1400 volts--where the counter ceases to be proportional--and 1600 volts--where the γ-ray counts become appreciable. It is desirable to operate on this count-rate plateau where the effects of power-supply voltage variation are reduced.

Gamma-Ray Counter

In the γ-counter (Fig. 40) scintillations of a sodium iodide crystal are observed with a type 6292 photomultiplier tube. Because the photomultiplier pulse is rather short and peaked, it is desirable to shape it before amplification. This shaping is done with the circuit shown in Fig. 41. Capacitor C_1 integrates the sharp pulse of current from the photomultiplier. To prevent this capacitor from remaining charged (and yet not produce the peaked pulse that would occur if a short time-constant RC circuit were used) a clipping line is introduced. The photomultiplier pulse charges the capacitor C_1 to voltage E_1 in less than 0.5 μsec. This voltage is impressed upon a network mainly consisting of R_1 and the Z_0 of the RG 65/U clipping line Z_1, Z_0 of which is about 950 ohms. Therefore a step of voltage of approximately $950E_1/1950$ is applied to the 6AH6 cathode follower. The pulse that travels down the clipping line is partially reflected and partially absorbed by R_2. The reflected portion returns and meets an impedance consisting of R_1 in series with C_1, which is near enough to the Z_0 of the line to prevent further reflections. By adjustment of R_2, the reflected portion can be made sufficient to just cancel any charge remaining on C_1. The resultant pulse applied to the cathode follower is fairly square, of about 0.5 μsec length, and of a height that is closely proportional to the net energy delivered to the crystal by the γ-ray. The cathode follower feeds the pulse to the signal lead to the linear amplifier.

Noise pickup in the photomultiplier is reduced by an electrostatic shield, which surrounds the tube and crystal and is connected to the first dynode (Pin #1). A magnetic shield is also desirable.

In order to reduce light reflections at the interface between crystal and photomultiplier tube, the space is filled with clear mineral oil.

Linear Amplifier

The linear amplifiers supply a voltage gain of 8,000 to 10,000 in the frequency range of 30 kc to 2 mc. The term linear refers to the voltage amplitude of output pulse relative to input pulse. The features that distinguish a good linear amplifier are:

(a) constant gain without regard to pulse height;

(b) constant gain without regard to tube age;

(c) constant gain without regard to power-supply voltage;

(d) constant gain without regard to equipment temperature;

(e) short rise and decay times without overshoot;

(f) abrupt saturation and rapid recovery on overloading pulses;

(g) useful linear range of pulse height to 90% of overloading point;

(h) pulse output on the order of 100 volts peak with noise of the order of 0.5 volt peak.

The linear amplifiers we used were weak in requirements (b), (c), and (d).

Pulse-Height Analyzer

The pulses from the slow-neutron detector counter or the γ-counter are sent to the pulse-height analyzer. The pulse-height analyzer accepts only those pulses which are higher than a certain adjustable "base line." It can also be made to accept only those pulses which exceed the base-line voltage by an amount that is less than that of the "window" width. The base line is adjustable from 0 to 70 volts and the window from 0 to 7 volts. As an example, if the base line is set to 35 volts and the window to 3 volts, only pulses between 35 and 38 volts high are accepted by the pulse-height analyzer. Each pulse that is accepted causes one pulse of fixed height to appear in the output of the pulse-height analyzer. With this device it is possible to analyze the γ-ray pulses from the scintillation counter to determine the γ-ray energy.

When the BF_3 slow-neutron counter is being used, the only requirement is that the equipment discriminate against γ-ray pulses from the BF_3 counter. Since the BF_3 counter works in the proportional region for γ-rays, but saturates with neutrons, the neutron pulses are much larger than the γ-ray pulses. The base-line control is set on the count-rate plateau of neutron pulses and the window control is set to maximum.

The pulse-height analyzer we used is a single-channel type (only one window). It is a Model 501 made by Atomic Instruments Co., Cambridge, Mass.

Scaler

The output pulses from the pulse-height analyzer are sent to two scalers and the output from the neutron monitor linear amplifier is sent to two other scalers having built-in discriminators which serve the same function as the base-line control of the pulse-height analyzer.

Because there are only certain periods of time following the pulse of the neutron source during which we can obtain useful information by counting the pulses, the scalers are provided with gated amplifiers which allow the pulses to be counted only when they are gated "on".

Tandem Scaler-Gating Unit

The tandem scaler-gating unit receives pulses from the trigger multivibrator at a 60-pulse-per-second rate. These pulses trigger the first of five one-shot multivibrators, which are connected in sequence so that each multivibrator, at the end of its "on" period, triggers the next. "Gates" are obtained from each multibivrator via cathode followers and are applied to the scalers. The gates are + 20 volts high and vary in length from 275 μsec to 8,333 μsec, as shown on the timing sequence chart (Fig. 42).

Stability Requirements

If we require an upper limit of 1% drift in count rate caused by equipment instability, we find the stability requirements for any one piece of equipment, with all others perfect, as follows (Table II):

Table II

Stability Requirements

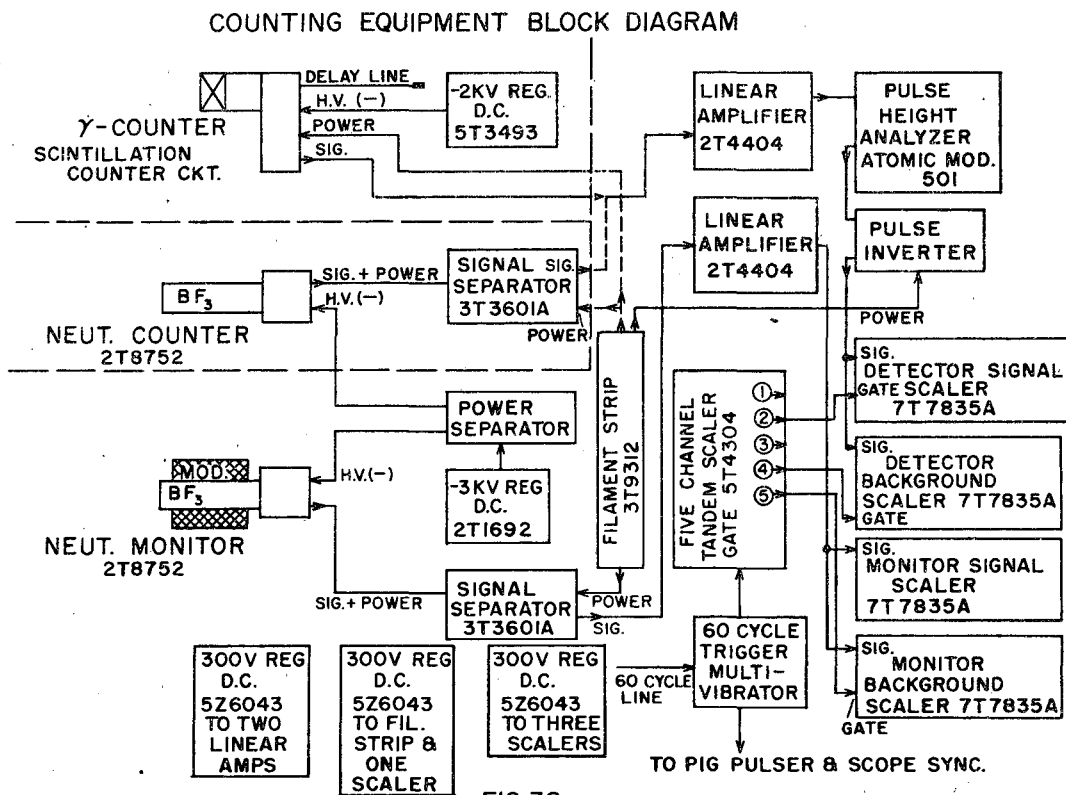| Equipment	Typical Operating Conditions	Requirement
BF$_3$ counter supply	On plateau 75 V wide in 1500 V	5% regulation
γ counter supply	500% gain change with 25% supply change 50% rate change for 10% gain change	0.01% regulation
γ linear amplifier	50% change in rate for 10% change in gain	0.2% gain stability
γ PHA base	50% change in rate for 10% change in voltage when used as a discriminator	0.2% voltage stability
γ PHA window	Linear for small changes	1% window width stability
Neutron scaler discriminator	10% change in rate for 20% change in voltage	2% voltage stability
Tandem scaler gates	#1 5 μsec in 275	2% time stability
	#2 6 μsec in 300	2% time stability
	#3 Not critical but must not allow gate 5 to overlap next Pig pulse	3% time stability
	#4 Low count rate--small effect	6% time stability
	#5 Low count rate--small effect but must not overlap next Pig pulse	2% time stability
Trigger multivibrator frequency	Consistent with overlap requirements of tandem scaler-gating unit	2% time stability
Linear amplifier power supplies	Consistent with linear amplifier requirements	~0.1%

COUNTING EQUIPMENT BLOCK DIAGRAM

FIG. 38

MU-8826

Fig. 38. Block diagram of counting equipment.

BF$_3$ NEUTRON COUNTER

1½" O.D. × 9" BRASS TUBE

.003" STAINLESS STEEL WIRE

GAS ADMISSION VALVE

CATHODE FOLLOWER BOX
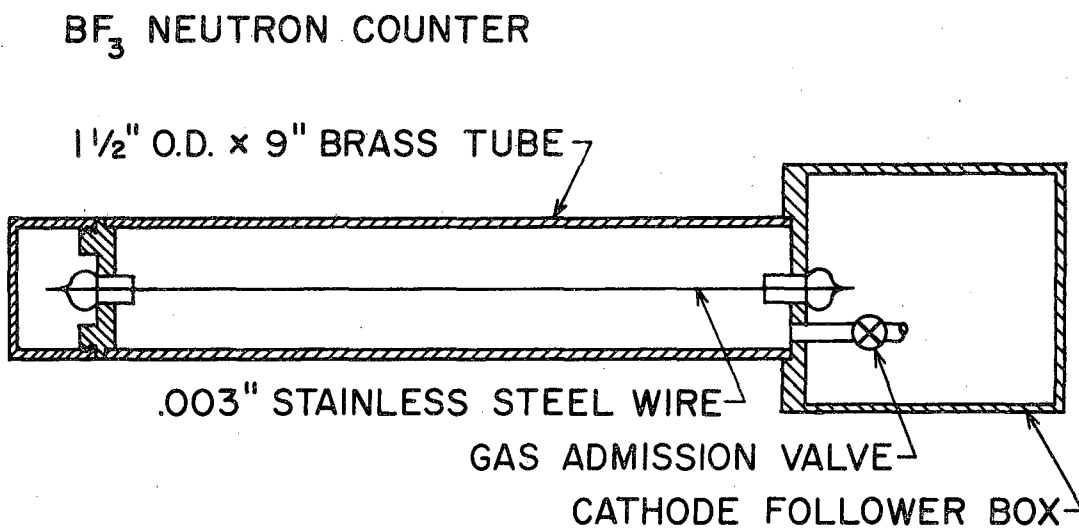
FIG. 39

MU-8798

Fig. 39. Diagram of BF$_3$ counter (physical).

γ – COUNTER

ALUMINUM   SODIUM IODIDE
CRYSTAL HOUSING   CRYSTAL
COTTON PACKING

BINDING
WIRE   MINERAL OIL
                                            FILM

ALUMINUM   6292
FOIL   PHOTOMULTIPLIER
ELECTRO-   TUBE
STATIC SHIELD

                                      BAKELITE
                                      HOUSING

BINDING
WIRE   MOUNTING
CONNECTED   RING
TO PIN #1

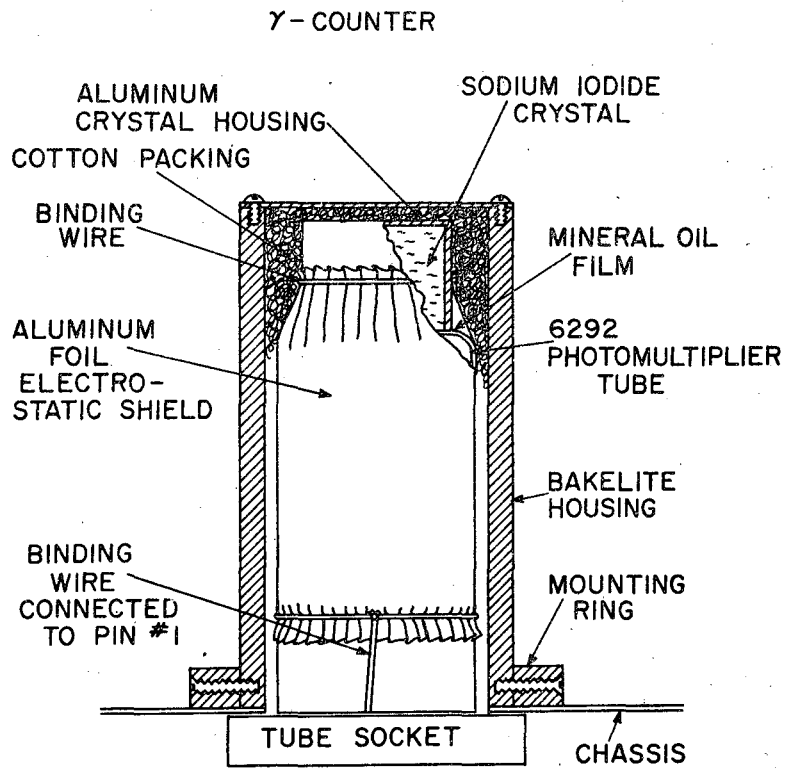TUBE SOCKET   CHASSIS

FIG. 40

MU-8827

Fig. 40.   Diagram of gamma counter (physical).

SCINTILLATION COUNTER CIRCUIT
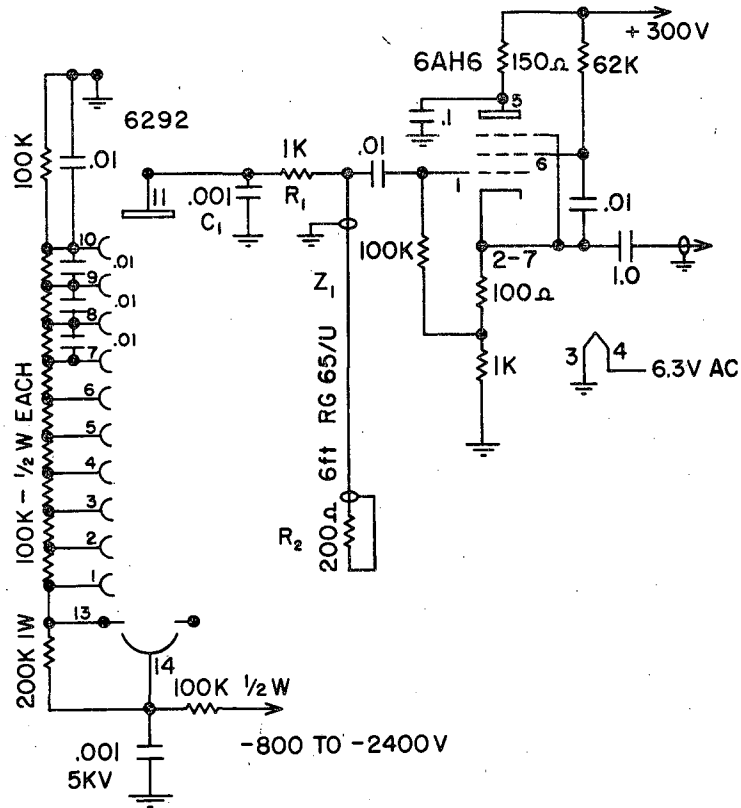
FIG. 41

MU-8828

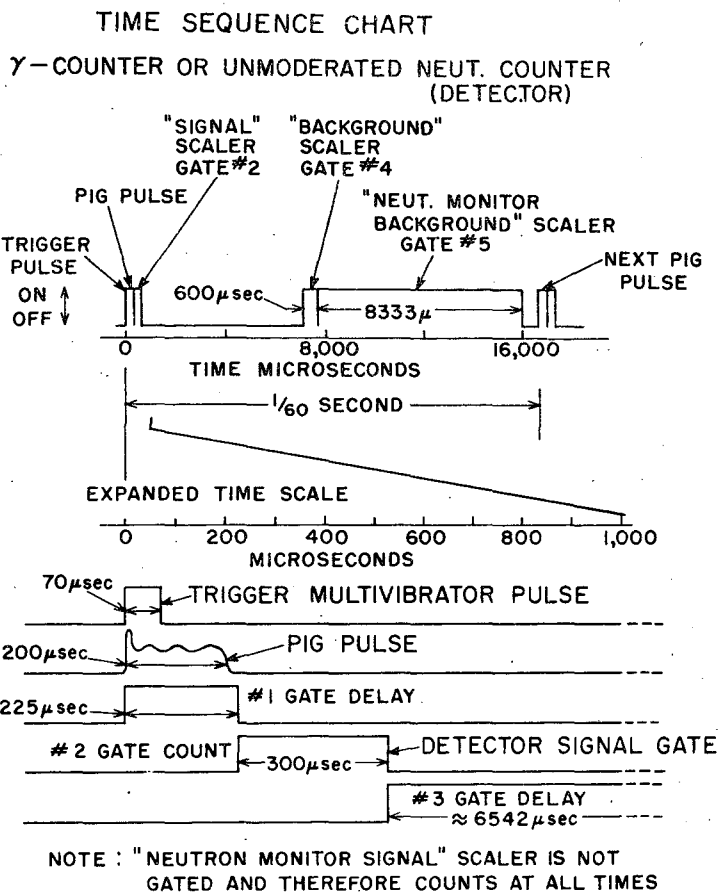Fig. 41. Diagram of gamma counter circuit.

TIME SEQUENCE CHART

γ−COUNTER OR UNMODERATED NEUT. COUNTER
(DETECTOR)

NOTE : "NEUTRON MONITOR SIGNAL" SCALER IS NOT
GATED AND THEREFORE COUNTS AT ALL TIMES

FIG. 42

MU-8829

Fig. 42.   Gating sequences.

III. A Sample Calculation

Knowns:

R_{TO} Counting rate with sample absent (counts/sec)

DR Ratio of $\dfrac{M_T \text{ (in)}}{M_T \text{ (out)}}$; Detection Ratio

M_T (in) = Ratio of number of counts from detector to machine flux (cts) with sample in.

M_T (out) = Ratio of number of counts from detector to number of flux (cts) with sample out.

Conditions:
(Chosen knowns)

What is choice of detection factor, DF?

Refer to graph of DF vs odds (Fig. 44).

(if DF = 4, odds against no detection = 150:1)

(if DF = 6, odds against no detection = 20,000:1)

You are obviously safer if the DF is 6.

Unknown:

Time, t. Amount of time required to fulfill the above conditions.

1st Step:

We know R_{TO}, DR and we have chosen DF = 6 (for instance)

Then: $f_{DR} = \dfrac{DR - 1}{(DF)\,DR}$

If DR = 1.2, then

$$f_{DR} = \frac{1.2 - 1}{6\,(1.2)} = 0.0278 \quad \text{or } 2.78\%$$

2nd Step:

We have

$$f_{DR}\,(R_{TO}\,t)^{1/2} = 0.67 \left(\frac{DR + 1}{DR}\right)^{1/2} = F(DR)$$

Refer to the graph of F(DR) vs DR (Fig. 43)

$$\left(\text{or calc. } \left(\frac{DR + 1}{DR}\right)^{1/2} 0.67\right)$$

We know R_{TO} (say 10 cts/sec), f_{DR} = 0.0278, and F(DR),

then $0.0278\,(10t)^{1/2} = 0.907$ $F(DR) = 0.67 \left(\dfrac{1.2 + 1}{1.2}\right)^{1/2} = 0.907$

$$t = \left(\frac{0.907}{0.0278}\right)^2 \frac{1}{10} = 106.5 \text{ sec}$$

We now know we can determine the presence of a mine in 106.5 sec with DR = 1.2, R_{TO} = 10 cts/sec, DF = 6 and a calculated f_{DR} of 0.0278. As mentioned above, the odds against missing this mine (a statistical miss) are 20,000:1.

DR is determined by measurement and is a function of the "earth", size of mine, etc.

R_{TO} is also determined by measurement and is a function of the number of counters, the efficiency of the counters, the type of "earth" the machine is looking at (no sample 'mine' present), and the flux from the machine.

DF is up to the designers. It is a function of time. The larger the DF the longer one must count over a given area but the safer the detection.

The area covered is a function of the shape of the counter array. It must be remembered that R_{TO} is the rate (cts/sec) from all the counters that are connected in parallel. The area covered, therefore, is a function of counter geometry only as discussed in the section on thermal neutrons.

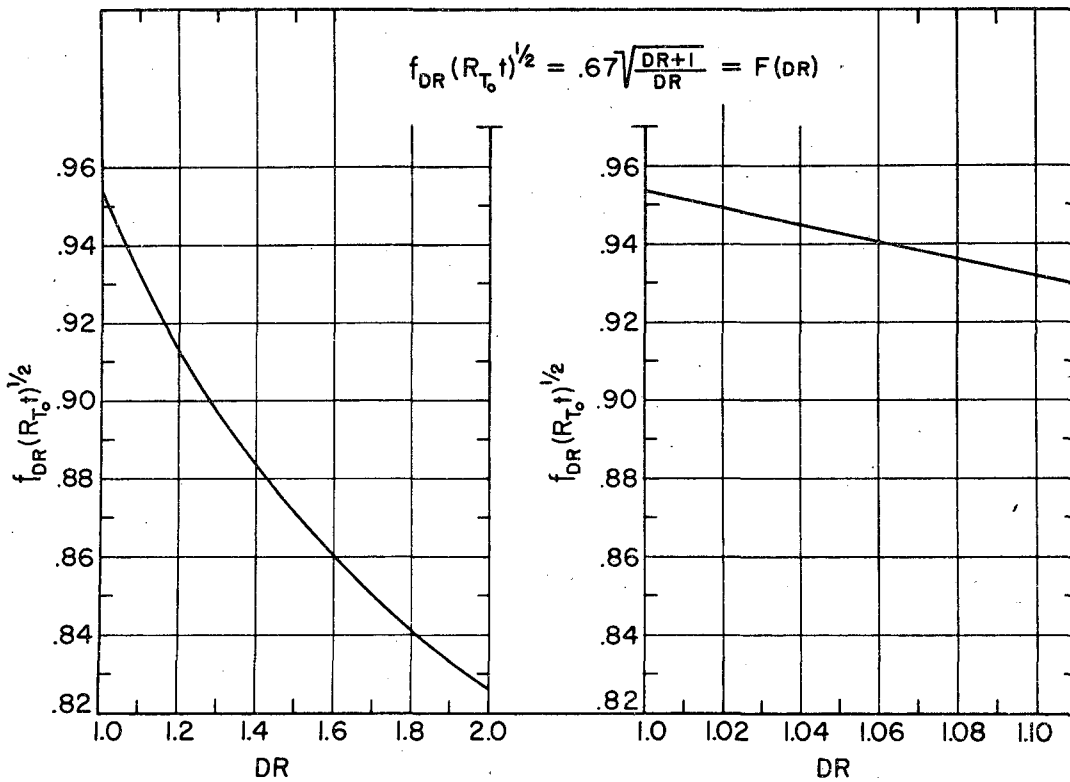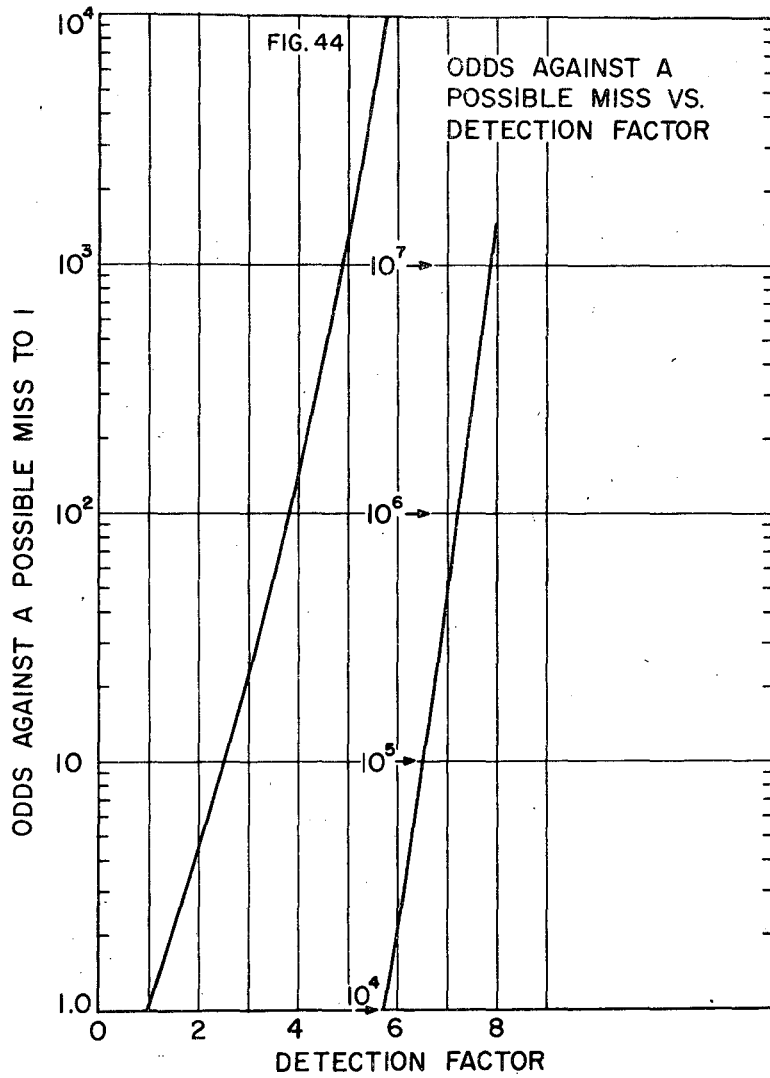$$f_{DR}(R_{T_o}t)^{1/2} = .67\sqrt{\frac{DR+1}{DR}} = F(DR)$$

FIG. 43

MU-8830

Fig. 43. Graph of $f_{DR}(R_{TO}t)^{1/2}$ vs DR (detection ratio).

MU-8831

Fig. 44. Graph of odds against a possible miss vs detection
    factor.